

Review of Mono- and Bifacial Photovoltaic Technologies: A Comparative Study

Tanvir M. Mahim[✉], Student Member, IEEE, A. H. M. A. Rahim[✉], Life Senior Member, IEEE, and M. Mosaddequr Rahman[✉], Senior Member, IEEE

Abstract—This article reviews the recent works on bifacial and monofacial photovoltaic (PV) technologies. Furthermore, the effectiveness of bifacial PV technologies over that of monofacial technologies is examined. Unlike monofacial PVs, bifacial PVs have light sensitivity on both the front as well as the rear surface and, therefore, have higher PV yield compared to monofacial PVs. However, because of higher energy output, thermal and electrical behavior are critical in bifacial PV, which needs to be optimized for bifacial PV cells to maintain the optimum cell efficiency. Studies show that bifacial thin-film Si-heterojunction PV cells have the maximum laboratory efficiency. Surface area, the fraction of light reflected, geographical location, economy, and efficiency are key contributing factors that govern the selection of bifacial PV systems. The dual use of land gives an edge to bifacial PV systems over monofacials. The dual use of land cases, such as agri-PVs with bifacial, vertical bifacial, and floating-PVs with bifacial, are unique systems where monofacial PV modules are less effective.

Index Terms—Agri-photovoltaic (PV) with bifacial, bifacial, bifaciality factor, floating-PV with bifacial, heterojunction cell, monofacial.

I. INTRODUCTION

THE major difference between bifacial and monofacial lies in how photovoltaic (PV) modules (panels) are installed to harness radiation on the back surface. The increased efficiency of bifacial PV cells is a result of applying high-efficiency concepts from monofacial PV cells. A high-efficiency monofacial PV cell with optimal surface passivation and high-quality substrate is a great bifacial PV cell [1], [2], [3]. A key factor for bifacial is two-faced light sensitivity. The thin-film category of Si-heterojunction (SHJ) PV cell shows maximum efficiency with minimal fabrication complexity [4], [5]. The passivated rear surface cells, such as p-type passivated emitter-rear [6], interdigitated backcontact (IBC) [1], and n-type passivated emitter-rear diffused [7] cells, are widely manufactured for bifacial PV panels. Here, the term passivated means to reduce the charge carrier's recombination loss with cell surface coating layers.

Manuscript received 25 November 2023; revised 11 January 2024; accepted 12 February 2024. Date of publication 14 March 2024; date of current version 19 April 2024. (Corresponding author: Tanvir M. Mahim.)

The authors are with the Department of Electrical and Electronic Engineering, Brac University, Dhaka 1212, Bangladesh (e-mail: tanvir.mahim@bracu.ac.bd; abu.hamed@bracu.ac.bd; mosadeq@bracu.ac.bd).

Color versions of one or more figures in this article are available at <https://doi.org/10.1109/JPHOTOV.2024.3366698>.

Digital Object Identifier 10.1109/JPHOTOV.2024.3366698

Panel designs for bifacial and monofacial are similar, except for a few design considerations. The bifacial panel's oversaturated current flow is contained using electrical design optimization [8]. It is done to optimize the voltage–current ratio of the cell. The optimization process uses half-cut cells, multibusbar, and multiwire concepts. Optical design consideration for bifacial minimizes PV cell-to-panel loss [9]. Thermal behavior is essential for bifacial PV panels because of their high current generation [4]. Optical, electrical, and thermal modeling of bifacial PV panels are necessary to optimize maximum output.

The differentiating factor for bifacial and monofacial PV systems is the bifaciality factor and bifacial gain [10], [11]. It shows the quantitative benefits of bifacial systems over monofacial ones. Conventional systems use monofacial PV but the development of the bifacial PV system has risen because of the dual use of land cases. Vertical bifacial [12], [13], agri-photovoltaics (agri-PVs) with bifacial [14], and floating-PVs with bifacial [15] PVs are dual use of land examples. Because of optimum energy production compared with fixed and dual-axis tracking [16], single-axis tracking [17] is used for bifacial rooftop systems.

The rest of this article is organized as follows. Section II discusses the conventional monofacial PV technologies. Section III explains the bifacial PV technologies. Section IV briefly explains the bifacial panel design considerations. Section V presents bifacial PV systems and their recent advancements. Section VI discusses the leveled cost of electricity for bifacial PV systems. Section VII provides the future of bifacial PV. Finally, Section VIII concludes this article.

II. CONVENTIONAL MONOFACIAL PV TECHNOLOGIES

The first-generation PV cell technology commercially used was crystalline cells [18]. The second generation is thin-film cells. Third-generation solar cells improve on first-generation silicon (Si) cells and second-generation thin-film cells. These cells typically employ unique technologies, such as multijunction designs, tandem topologies, or new materials, such as perovskites and organic semiconductors, to boost efficiency and broaden the absorption spectrum. These are aimed at increasing the efficiencies of single-bandgap devices and decreasing time-intensive fabrication processes [19]. Laboratory thin-film cells achieved a conversion efficiency of nearly 20% using non-single-crystal structures [20]. The losses were because of limitations to carrier performance mobilities. A minimal amount of material is required in such cell technology. Wafer thickness

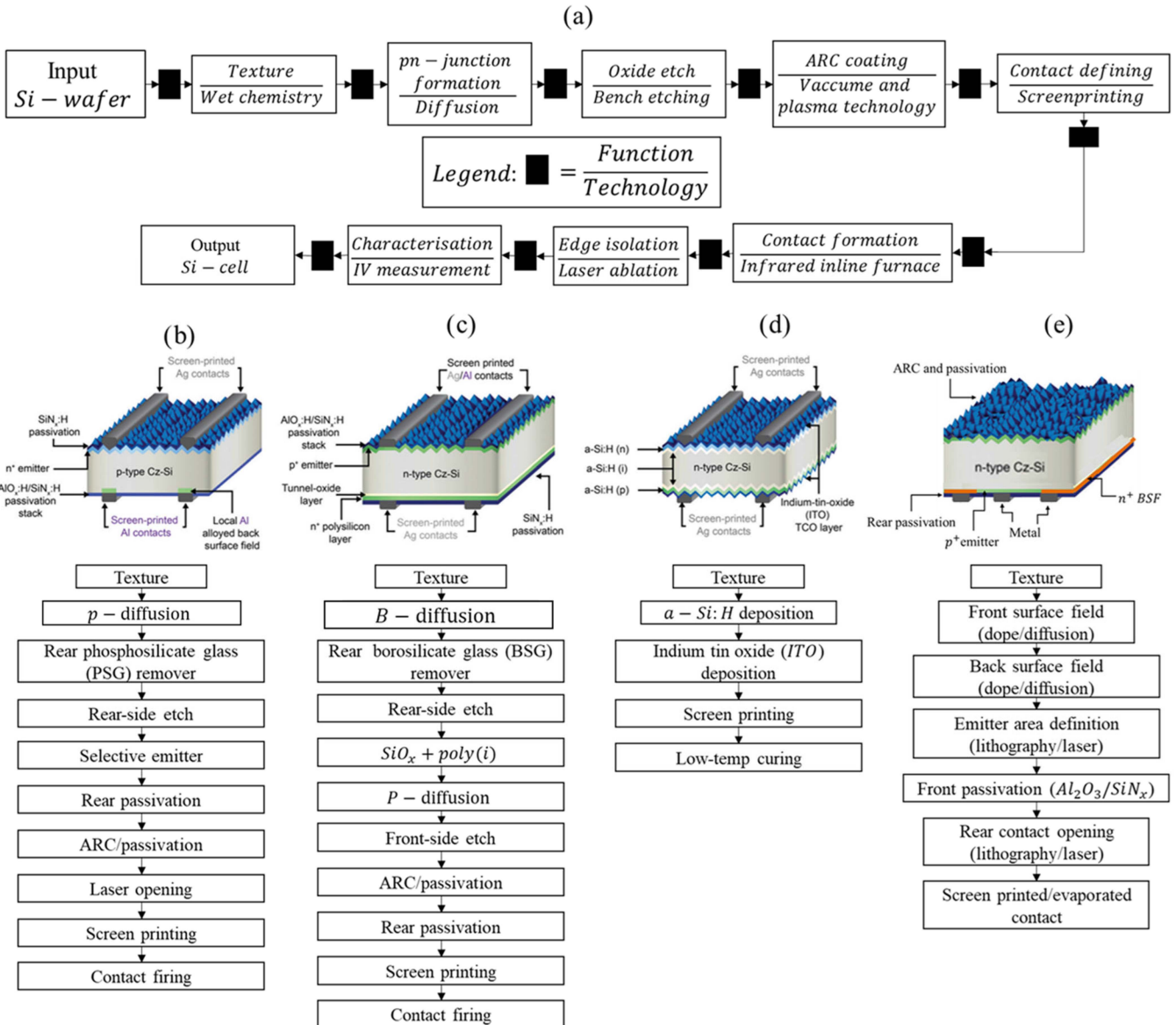


Fig. 1. (a) Industrial Si-cell fabrication diagram. Cell schematic-fabrication diagram: (b) PERC, (c) TOPCon, (d) SHJ, and (e) IBC.

is needed to be at (1–2) μm to deposit thin film fabrication. The materials approach photon current saturation within this range. However, crystalline silicon (c-Si) needs a large width for photon absorption. The types of thin-film PV cells are amorphous silicon (a-Si), cadmium telluride (CdTe), and copper–indium–gallium–diselenide (CIGS). The gallium arsenide (GaAs) is a cell material with high efficiency. The availability of indium is the limiting factor in thin-film materials. It is because of copper indium diselenide cells [21]. Knapp and Gay [22] showed the correlation between optical wavelength and photocurrent density for thin-film PV cells and compared them with c-Si and showed the saturation point occurrence for thin-film cells with optimum photocurrent density [23].

Fig. 1(a) depicts the industrial Si-cell fabrication process [24], [25]. The process varies based on the cell technology that is intended. The mainstream monofacial c-Si PV cells are

passivated emitter and rear cell (PERC), tunnel oxide passivating contact (TOPCon), SHJ, and IBC [26]. Fig. 1(b)–(e) provides the schematics and fabrication process for the mainstream c-Si PV cell technologies [27], [28]. Fig. 1 shows that the deposition of ARC/passivation layers is a key step among the c-Si PV cell configurations. The most commonly used process for manufacturing ARC/passivation layers is chemical vapor deposition (CVD), specifically plasma-enhanced chemical vapor deposition (PECVD), low-pressure chemical vapor deposition (LPCVD), and atomic layer deposition (ALD). The primary technology for indium tin oxide layers in SHJ PV cells is physical vapor deposition (PVD) sputtering. The vapor states are what distinguishes PVD from CVD. In PVD, the vapor is made up of atoms and molecules that condense on the substrate; in CVD, the vapor conducts a chemical reaction on the substrate, resulting in a thin film [29]. Despite the fact that the

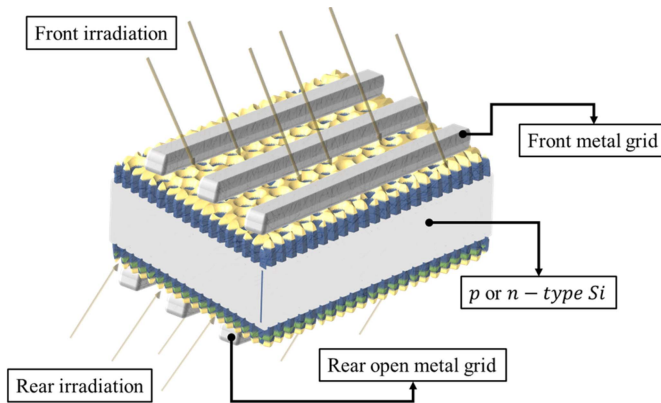


Fig. 2. Typical bifacial cell scheme.

process often requires corrosive gases, CVD films offer higher quality in terms of high purity and density, as well as better coverage on difficult surfaces than PVD films [30]. PECVD is a popular method for depositing thin films in the production of c-Si PV cells. On PERC and TOPCon PV cells, the current fabrication method uses PECVD-produced Si nitride (SiN_x) as a front-side antireflection layer. PECVD $\text{SiN}_x:\text{H}$ coated with PECVD or ALD AlO_x provides excellent passivation and is commonly utilized in the fabrication of PERC and TOPCon [31], [32]. LPCVD dominates the manufacture of polycrystalline Si (poly-Si) for TOPCon PV cells in the PV market. However, in order to reduce costs, LPCVD technological challenges such as higher deposition temperatures, reduced deposition rates, and wrap-around deposition issues that increase production energy consumption must be overcome [33], [34].

Bifacial cells use transparent substrates, compatible with the fabrication of the front and rear p-n junctions. For monofacial cells, the p-n junction is fabricated on the front side. It involves the diffusion of (dopants) boron and phosphorus to the Si wafer and needs annealing to activate dopants. Bifacial cell fabrication of a front-side p-n junction is similar to monofacial cells, where rear-side transparency and reflection are the additional aspects [35]. The front-side antireflection coating is crucial for optimizing front-side light capture for mono- and bifacial. In monofacial cells, a reflective layer covers the rear side to prevent photons from escaping. The rear surface has metal contacts for electrical connectivity. However, bifacial cells are designed for photons reaching the rear side [36]. A lightly textured surface is included at the rear side. The rear surface has metal contacts and a rear-emitter design to maximize light collection. Group III elements form a strong bond that remains stable under heat cycling. It acts as a p-type donor, resulting in a heavily doped product. A severely doped p-region produces an impurity gradient, which causes an electric field to force holes back into contact [37]. The front-contact is opaque to light that blocks photons from entering the cell. The area of the front-contact is lessened for the absorption-deducing process of photons. Besides, the resistance of the contact increases for a small area of the front-contact. This is because of the proximity of the connection to the front surface. Annealing the contact material causes it to infiltrate into Si and shorten the connection [7]. As the current in the

contacts increases, so must the cross-sectional area of the contacts. It allows the contact to resist overall current limitations because of voltage loss. Monofacials contain metal gridlines made of Ag and Al, which are imposed on the front surface. It acts as an electrical conductor which forms a grid pattern. It permits light to travel through and reach the semiconductor material's front surface. The emitter region of the front-side cell allows the separation and collects electron–hole pairs generated through solar irradiance. However, bifacial cells have an additional set of contacts on the rear side to collect electrons [38]. For bifacial, rear metal gridlines are applied to the rear surface. Its purpose is to allow light to penetrate through the back surface and reach the rear-emitter portion of the cell. Bifacial cell's rear-emitter region is heavily doped. It acts as a separate p–n junction on the rear side allowing electron–hole pair separation and collection on the rear side [39].

III. BIFACIAL PV TECHNOLOGIES

Bifacial PV cells have partially metallized backside. As seen in Fig. 2, bifacials effectively respond to light from the front and back sides. Most production-level PV cells are p-type Si cells [40]. A bifacial panel is simply a monofacial PV module made with bifacial cells. It is structured with a reflecting sheet, a substance between and behind the cells. Transmitted illumination gets absorbed toward the cells, increasing the efficiency of the panel [41], [42]. A transparent back cover is used to integrate bifacial cells into a panel. They are based on glass or transparent foil. The bifacial panels produce higher energy output than standard monofacial panels. It is because of the extra energy created by rear irradiation [43].

The original technique for creating a bifacial cell was building a p^+np^+ structure by creating a p^+ junction on both surfaces of an n-type Si-wafer [44], [45].

Zhao et al. [46] fabricated front and rear p-n junctions in bifacial GaAs PV cells, where the twin junction design increases the efficiency of long-wavelength photon gathering. It was done to avoid restricting solar cell efficiency because of minority carrier diffusion durations in bulk Si. In this context, forming a connection on both surfaces increases surface passivation. The primary benefits of n^+ , pn^+ or p^+ , and np^+ structures were improved photon collecting effectiveness and used for long-wavelength photons as well as surface passivation [47], [48]. A back-surface field (BSF) with a similar doping-type base material reduces recombination and improves the V_{oc} [49], [50]. The challenge of collecting carriers at the back surface resulted in physical mechanisms for surface and bulk recombination. Many of today's sophisticated PV cell designs with passivated rear surfaces, such as p-type passivated emitter and rear contact cell (p-PERC), IBC cell, and n-type passivated emitter rear totally-diffused (n-PERT), evolved together with bifacial PV cells [7], [38].

Bifacial and monofacial cells in the same panel setup in a high-albedo site found that the short-circuit current J_{sc} ratio between the two was consistently close to 1.45 [51], [52], [53]. A ratio of 1.55 was found to be significantly higher in the early morning or on cloudy days [51], [54]. Based on panel output

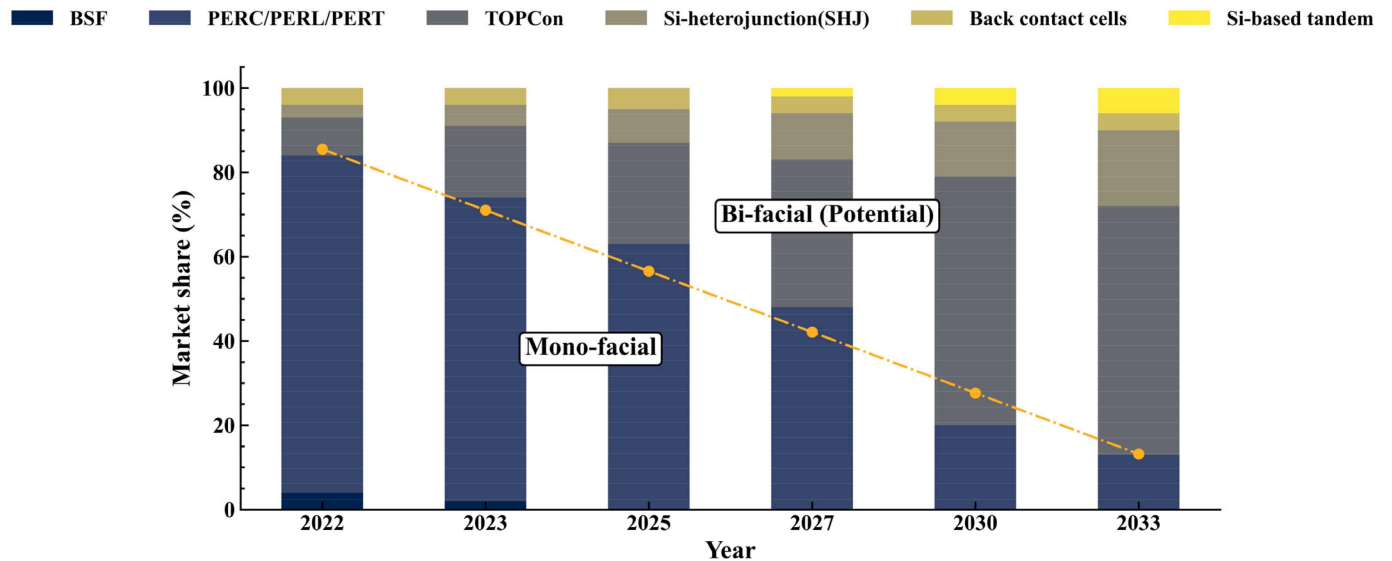


Fig. 3. ITRPV technology share projection: World market share for numerous cell technologies.

powers, a bifacial panel would generate approximately 50% more electrical power than a conventional monofacial panel [55]. The rear-side recombination of the backside surface and the lifetime in p-type Cz or multi-crystalline material were the constraints of p-type aluminum back-surface field (Al-BSF) PV cells. Thus, overcoming recombination on the backside was necessary to improve efficiency. This leads to cells with a PERC. The backside is protected by a dielectric layer, with just local aluminum (Al) connections [6], [56]. To bypass the bulk lifetime constraints, a method was to use an n-type base material. The n-type has a longer lifetime and is less susceptible to metal impurities than the p-type [57], [58]. As a result, it is used in high-efficiency cell designs such as n-type heterojunction or IBC PV cells.

Fig. 3 depicts the expected share of various technologies till 2033 [59]. The TOPCon technology has the prospect to gain a 60% market share by 2033 while all other technologies have been bifacialized. The “PERX”-PERC, PERT, and PERL technology dominate the market. It is determined by n-type structures that which technology will dominate. It also depends on the market impact of bifaciality and how carrier-selective contacts are implemented. Similar to back contact concepts, SHJ technology has an 18% market share. IBC and supertandem technologies are gaining popularity. Perovskites, GaAs nanowires, and CIGS are supertandem PV cells that are mounted on a c-Si PV cell. The devices are bifacial with front-side efficiencies exceeding 30% [59].

A. Bifaciality Factor

The bifaciality factor is an essential parameter of a bifacial device [60]. It denotes the proportion of the device’s rear and front responses. A panel’s bifaciality factor is used to calculate the additional energy generated by rear irradiance. For current density J_{sc} , voltage V_{oc} , power, and efficiency, the bifaciality

factor [61], [62]

$$\varphi_{J_{sc}} = \frac{J_{sc_r}}{J_{sc_f}} \quad (1)$$

$$\varphi_{V_{oc}} = \frac{V_{oc_r}}{V_{oc_f}} \quad (2)$$

$$\varphi_{P_{max}} = \frac{P_{max_r}}{P_{max_f}}. \quad (3)$$

Here, J_{scf} and J_{scr} represent the short-circuit current density for the front and rear sides at standard test conditions (STCs) under single-sided illumination, respectively. Stray light on the dark side makes measuring the front and rear $I-V$ characteristics of bifacial cells problematic [63].

The parameters that determine the bifaciality factor contain the rear surface texture, an antireflection coating, metal coverage as well as doping-passivation on the backside, and base resistivity. The first three features influence light coupling into the cell, which results in the formation of charge carriers. The remaining variables determine whether charge carriers recombine or are collected at the electrodes, contributing to the creation of electricity [64]. The texture and antireflective coating on the back J_{sc} are similar to those on the front. The texture and antireflective coating are optimized for a low reflection and optimal light coupling to maximize the bifaciality factor and increase the rear J_{scr} . It should be done without compromising the rear surface passivation by lowering the front-side short-circuit current J_{scf} . Typically, the optimization of the parameters results in a varied texture on the front and back surfaces [10]. Bifacial cells are metallized in an H-pattern and have three to six busbars and fingers. Balanced recombination losses at the contacts, shading losses for rear-side lighting, resistive losses, and silver paste consumption define the number and width of the fingers and busbars on the rear-side metal grid. The metallization fraction on the rear influences the rear current J_{scr} . Resistive losses in Si affect the grid’s fill factor (FF), contact resistance, and lateral

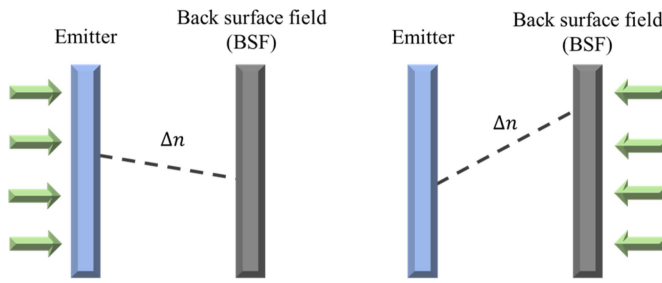


Fig. 4. Gradient in carrier concentration of bifacial PV cell for the front (left) and rear (right) irradiance.

conductivity. Recombination at the contact harms both V_{oc} and FF [65], [66]. Passivation and conduction are optimized in the BSF. It is done to supplement the base's lateral conductivity.

To compensate for the conductivity of a significant path length, the doping level must be increased if the partial metallization at the rear has a bigger pitch. At the back, the J_{sc} is susceptible to surface recombination. It is more common in cells with a front-side junction, and it also contributes to auger recombination in the back. Auger recombination is a nonradiative mechanism that transfers excess energy from electron–hole recombination to electrons or holes that are stimulated to higher energy levels within the same band rather than emitting photons [72].

The schematic for the more substantial gradient of excess carrier concentration Δn and average excess carrier concentration under rear illumination is shown in Fig. 4. High Δn at the back causes an increase in the recombination current J_{recomb} at BSF. J_{recomb} is affected by both the doping concentration N_d and the excess concentration Δn in the base material at BSF [73]

$$J_{recomb} = J_{0_{BSF}} \frac{(N_D + \Delta n) \Delta n}{n_i^2}. \quad (4)$$

Here $J_{0_{BSF}}$ is the recombination parameter of the BSF. Under back illumination on the emitter side, recombination is reduced. The difference in Δn between the front and back illumination at the emitter is substantially lower than at the BSF. A higher doping concentration equates to a lower base resistance ($N_D \sim 1/\rho$). At short-circuit conditions $\Delta n \ll N_D$, the recombination increases with decreasing resistivity [73]. Bifacial PV cell design is similar to monofacial cell design in that it is determined by the base material (p-type or n-type), junction creation, and metallization. As a result, bifacial variants of monofacial cell concepts, such as heterojunction, n-PERT, PERC+, and IBC cells, have emerged. The design of each type of bifacial PV cell is determined by the connectivity technology, number of busbars, and cost optimization [74].

B. Bifacial Heterojunction PV Cell

Bifacial SHJ PV cells (see Fig. 5) have the advantage of combining high efficiency with a small number of manufacturing steps. It has the potential for cells with conversion efficiencies greater than 25% [5], [75]. Furthermore, it has a low-temperature coefficient of open-circuit voltage (V_{oc}) ($-0.3\text{%/}^\circ\text{C}$) and a high

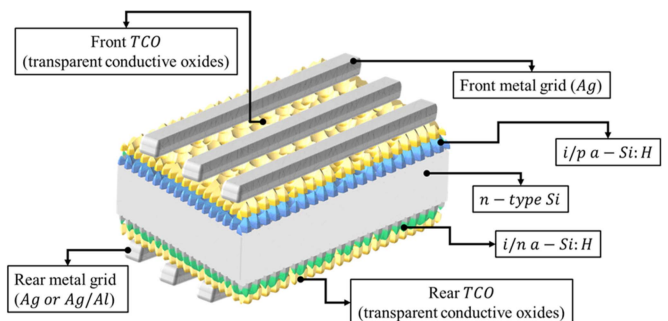


Fig. 5. Bifacial SHJ cell layout.

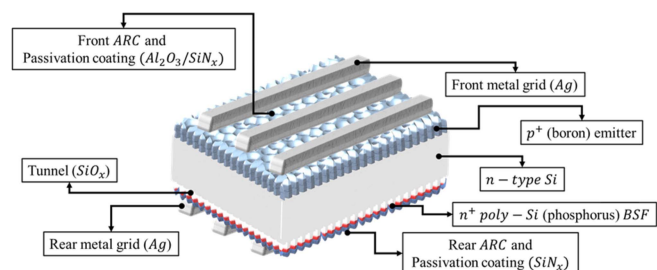


Fig. 6. Bifacial TOPCon cell layout.

bifaciality (>92%), resulting in a high energy yield for bifacial heterojunction modules [75], [76].

Han et al. developed bifacial heterojunction cells with reduced transparent conducting oxide (TCO) thickness. They presented three types of In_2O_3 -based TCOs, tin-doped, fluorine-doped, and tungsten-doped In_2O_3 , as well as minimized thickness [5]. From materials to devices, Liu et al. assessed the current state of research on high-efficiency c-Si heterojunction PV cells. They principally showcased SHJ technology based on hydrogenated amorphous Si (a-Si:H), poly-Si, and dopant-free passivating contact technology based on metal compounds as well as organic materials [77], [78].

C. Bifacial TOPCon PV Cell

TOPCon is an efficient n-type Si cell technology (see Fig. 6). It is constructed on an n-type Si substrate with a thin tunneling oxide layer applied before an extra layer composed of heavily doped n or p poly-Si that links the metal at both ends. As these restrict one type of carrier, such tunneling oxide contacts are referred to as passivating contacts [79]. The TOPCon bifacial cell efficiency ranges between 22% and 25% [68], [80]. Wang et al. [81] proposed high-efficiency n-TOPCon bifacial cells with selective poly-Si-based passivating contacts. Sen et al. [82] presented accelerated damp-heat testing at the of bifacial Si-TOPCon cells using sodium chloride.

D. Bifacial n-PERT PV Cell

The PERT cell design based on n-type material (see Fig. 7) offers easy-to-manufacture bifacial solar cells with high bifaciality and front cell efficiencies between 21% and 22% [83].

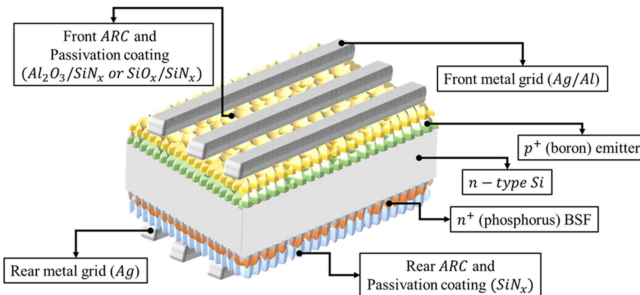


Fig. 7. Bifacial n-PERT cell layout.

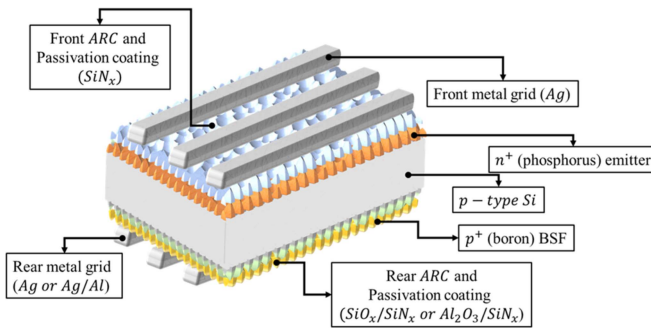


Fig. 8. Bifacial p-PERT cell layout.

The concept is easy to impose in p-type PV cell manufacturing processes [83]. Nakamura et al. [84] created the front junction bifacial n-PERT cells on thin wafers to examine the effects of wafer thinning on cell performance. Luo et al. researched potential-induced deterioration (PID) in the glass–glass n-PERT bifacial c-Si PV modules. They proposed that PID advancement is highly influenced by bias voltage and stress temperature [85].

E. Bifacial p-PERT PV Cell

The resistance of p-type Si to high-energy space radiation compared with n-type Si was the primary factor in p-type Si taking the lead in the PV sector for terrestrial applications (see Fig. 8) [39], [86]. On multi-c-Si, p-PERT PV cells were examined as an alternative to single-face PERC cells. Lohmuller et al. [35] exhibited 88% bifaciality for 6-in bifacial p-type Cz-Si passivated emitter and rear cells (bi-PERC) and increased their rear-side energy conversion efficiency to 18% through minimal manufacturing procedure changes. Fichtner et al. reported on the gettering efficacy of a technique that used doped glasses deposited before diffusion by air pressure chemical vapor deposition (APCVD). They hypothesized that uniform sheet resistances and doping profiles are suitable for creating inexpensive commercial APCVD-based codiffusion passivated emitter and backside diffused cell technology [87].

F. Bifacial p-PERC+ PV Cell

Bifacial PERC+ PV cells are made in the same manner as standard monofacial PERC cells produced by leading PV cell manufacturers. Monofacial PERC cells currently account for

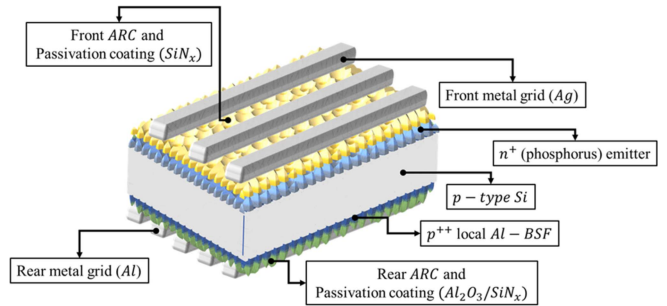


Fig. 9. Bifacial p-PERC+ cell layout.

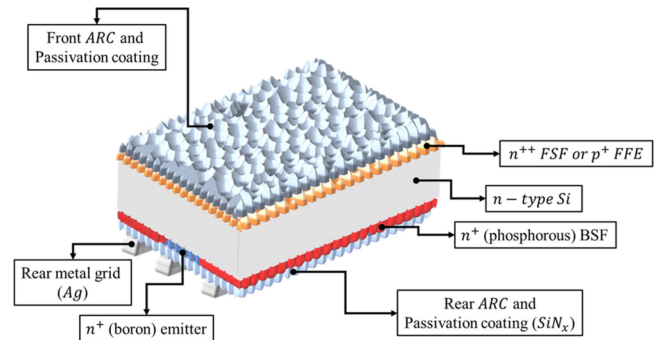


Fig. 10. Bifacial IBC cell layout.

80% of worldwide production capacity however it is expected to decrease because of the popularity of TOPCon cells. Around 13% market share for bifacial ones in the next decade is expected for PERC cells [59]. The Al-screen-print is changed from a full-area to an H-pattern design, and the depth of the rear-side passivation coating is adjusted for antireflective qualities that convert a monofacial PERC cell fabrication method into a bifacial PERC+ cell [88].

A PERC+ PV cell's cross-section layout is shown in Fig. 9. The PERC+ cell offers a path toward bifacial PV cell fabrication for monofacial PERC cell [88]. It is because of feasible production from monofacial PERC. In 2015, ISFH and SolarWorld began developing a bifacial PERC cell design independently, and later cooperatively, by using a screen-printed rear Al finger grid. It avoided the full-area Al-rear layer. It used an identical PERC fabrication process, with minor changes for rear passivation, and printing Al screen [2].

G. Bifacial Back Contact PV Cell

The metal electrode polarities on the backside of the IBC-Si PV cells (see Fig. 10) are visible. It provides benefits over traditional contacting cells. A few examples include the front-side shading loss absence, the possibility of wide coverage of backside grid metal, and the potential for a simple coplanar connector layout [89]. The cell layout is adjusted for front-side illumination of IBC PV cells and is manufactured using a variety of technologies, ranging from high-efficiency minimal-dimension processes to large-area conventional module cells [89]. Kim and Shafarman [90] demonstrated a CIGS-based

PV cell structure, which is a bifacial layout and a back-wall design. Edoff et al. [91] discovered an effect of passivation that increases the current density of cells having passivation. To overcome the energy mismatch band, Farrell et al. investigated innovative back-contact film layers. They discovered the optimal metasurface and electrical structures and the interfacial diffusion of elements [92].

IV. PANEL DESIGN CONSIDERATIONS FOR BIFACIAL PV

Bifacial panels have the potential to be used in large PV facilities as well as on residential flat-white roofs. It provides the possibility of investigating unique PV application possibilities, such as sound barriers and vertical installations [100]. The objective is to exploit the bifacial benefit for plants, such as a significant reduction of levelized cost of electricity (LCOE) with an optimum investment [101]. Optimization is concerned with the availability of backside irradiation with the light reaching the rear side of a bifacial panel. It is difficult to achieve light nonuniformity throughout the entire panel backside because of diffused and reflected indirect irradiance from the back-side. When the panel height above ground is increased, the rear-side homogeneity improves [102]. With diffuse irradiation, shadowing on the backside, such as mounting structures, has less of an influence than on the front side. It is subjected to direct illumination. The most apparent choice for bifacial panels is a glass/glass construction. These panels can function without a panel frame. They reduce the panel and balance of system costs by using mounting clamps. Frameless panels contain minimal sensitivity to the self-shading of the panel edge. Because of performance decline, soiling typically collects along the frame. It obstructs the natural drainage of the soiling layer. The glass/glass panel architecture, by definition, increases the structural load of the cell. It is because of the cells located on the panel's flat structural axis. In this regard, tensile stress, which causes cell cracking, is not applied. A glass backside, as opposed to polymer back sheets, acts as a humidity barrier. A double-glass structure reduces the weight of the panel. Besides, thermally tempered glass has a thickness of 2 mm [103]. A panel with a 2 mm front and back side has a structural as well as chemical durability advantage over a glass/back panel. It has a 4 mm [104] front cover without added weight to the panel. Furthermore, translucent back sheets enable the construction of lightweight bifacial panels [104].

The junction box design and its location are the most difficult challenges for a bifacial PV panel. Placing connection boxes on light-sensitive portions of the backside results in unwanted shadowing. The junction box is lowered in size or located near the panel's edge to keep the panel size constant. Because of the current created by the panel backside, the smaller junction boxes take higher currents [105]. By splitting the cells in half, the problem is solved. It reduces cell current and resistive losses, improving cell-to-panel performance [105]. Bifacial PV panels are useful for rooftops, building-integrated PVs (BIPVs), and urban applications. Non-standard-vertical installation designs provide energy production regardless of orientation. The design is implemented by using partially transparent panels with larger

cell spacing [14]. It gives daylighting while also reducing self-shading [14].

A. Bifacial PV Cell-to-Module (CTM) (Panel) Loss

The PV cells suffer losses throughout the panel construction process. Encapsulation affects the optical performance of the cell. PV cell coupling causes losses that impair the electrical performance of the panel. Because of the loss in the breakdown process, the panel power is less than the collective energy. The variance between entire cell power and panel power is referred to as CTM power loss. Losses in standard monofacial cells have been extensively studied [106], [107], [108]; however, bifacial ones need more extensive study relating to panel losses. CTM loss can be characterized as optical, resistive, and mismatched degradation.

Bifacial cells transmit radiation in the wavelength range of (900–1200) nm [109]. As a result, extra caution is necessary while measuring cells to optimize error for current measurement. Measuring bifacial cells on reflecting and nonreflective chucks results in differing cell current values, which are known as optical losses. In this regard, long-wavelength light enters the cell that is directed to the cell and affected by chuck reflectivity. Traditional monofacial measurement chucks are gold-plated and shiny. When compared with nonreflective chuck measurements, chuck reflectance adds to a 1% overestimation of cell current [109], [110]. A nonreflective background is used to measure bifacial panels. If the cells are tested with a reflecting chuck and the panel is measured with a nonreflective backdrop, the current-matched tandem (CTM) optical loss for bifacial panels is overestimated. To do an accurate CMT analysis, bifacial cells must be measured with a nonreflective chuck [111]. The resistive parts used to connect the PV cells cause a resistive loss in a wafer-based PV panel. Additional series resistance in the decentralization process is generated by parts such as the soldering ribbon, bussing ribbon, and contact resistance between the cell bus bar and the junction box. Because of background albedo, bifacial panels draw more current in real-world situations [112] and the resistive loss is proportional to the operating current squared. It is a major concern with bifacial panels. The current flow pattern in bifacial cells differs from that of monofacial cells. The ribbon's effective resistance for bifacial cells is more than for monofacial cells using traditional Al-BSF. It is because of differing metallization patterns on the cell's backside [54], [113]. As a result, when bifacial cells are integrated into panels, they have a larger resistive loss than monofacial cells.

B. Optical Panel Design With Bifacial PV Cells Scheme

Two different panel architectures enclose bifacial PV cells. One is glass/glass, while the other is nontransparent glass/back sheet [114]. When utilized with bifacial PV cells, both panel configurations have distinct advantages and disadvantages. The bifacial cells contained in the bifacial structure absorb albedo from the back of the panel using clear rear glass. When compared with a monofacial panel, it efficiently increases the energy yield. Because of a lack of acceptable measurement standards, the benefit is not reflected in STC measurements. Most panel

manufacturers measure bifacial glass/glass modules using only front-side light and a nonreflective cover on the backside [114], [115]. The partial transparency of bifacial panels is an important consideration. It modifies Yusufoglu et al.'s [116] proposed self-shading fix. The degree of transparency is influenced by factors such as cell-to-cell spacing and the optical properties of both glass panels. The transparency of bifacial PV panels is limited (5%–10%) [116]. When partial transparency is not used, the share of ground-reflected light to rear irradiance because of self-shading remains (90%–95%) of the total [117], [118].

While both monofacial and bifacial PV panels have comparable considerations for increasing light absorption and minimizing reflection, bifacial panels add the complexity of absorbing light from both sides. Bifacial gain and albedo are essential variables in the optical design of bifacial panels, making them more adaptive in specific deployment scenarios, especially when placed in areas with high ground reflectance. Monofacial panels are designed to absorb and reflect as much sunlight as possible from the front side. The optical design promotes sunlight absorption while lowering reflection in the active layers of PV cells. To reduce reflection losses, monofacial panels commonly use antireflection coatings on the front surface. These coatings are designed to lower the amount of light reflected off the surface, allowing more light to pass through and be absorbed by the PV cells. To capture sunlight, bifacial panels require an adequate optical design on the front side. Antireflection coatings and surface texturing can improve light absorption. Bifacial panels are distinguished by the fact that they gather light from both the front and back of the panel. One of the optical issues is the design of the rear surface to efficiently reflect and guide sunlight to the active layer. A reflecting material or coating on the back surface aids in light capture. Bifacial panels can also benefit from light reflected off the ground (albedo). The optical design considers the albedo of the ground surface, and the panel's direction and height above the ground are selected to capture reflected sunlight. For light to reach the backside of bifacial panels, the backsheet needs to be translucent. Backsheets that are transparent or have specific optical qualities can be used. Optical simulation methods are commonly used to predict bifacial gain while accounting for panel tilt, albedo, and ground cover. This contributes to the optimization of the design for maximum energy yield. Tracking devices that follow the path of the sun can greatly help bifacial panels. A tracking system's optical design tries to maximize the exposure of both the front and back sides of the panels to sunlight throughout the day. Julien et al. [119] proposed backside light management of four-terminal bifacial perovskite/Si-tandem PV panels considering realistic conditions. Yin et al. [120] presented optical enhanced effects on the electrical performance and energy yield of bifacial PV panels. Cote et al. [121] evaluated light management in bifacial PV with spectrally selective mirrors.

C. Electrical Design for Bifacial PV Cells Scheme

Traditional PV panels made up of bifacial PERC+ or n-PERT PV cells connect in the same way that monofacial PV panels do. An H-pattern metal grid is used to metalize the PV cells

on both the front and back sides [8]. Metal fingers collect photocurrent from Si wafers and transport it to busbars. To build an electrical contact between the front of a PV cell, Cu tabs with solder plating are joined to busbars. When comparing a PV panel to a naked PV cell, resistive losses in the cell-to-cell connections take precedence. The losses are proportional to the series resistance of the connecting tab multiplied by the square of the current. The current is affected by the coloration of the metallization grid and the connecting components. The interconnection material determines the series resistance, number of interconnecting parts, and cross section. Because of the double-sided lighting of the panels, bifacial panels generate more current [8]. The multibusbar interconnection is a scheme where round wires replace rectangular tabs. The wires reduce the contact area between the cell's metallization and the linking material, allowing no busbars to be used. According to the manufacturer, the wires reduce the reflection losses associated with flat tabs, hence enhancing light capture. Companies are promoting these multibusbar linking solutions. Schmid pioneered the multiwire technique [122], and Yao et al. [123] developed the *SmartWire* technology as pioneered by *Day4Energy* [124].

To minimize resistive losses in cell-to-cell interaction, the transport current must be reduced. At constant current density, reducing cells by half and three-quarters reduces the overall current per cell by 50% and 30%, respectively [125]. It lowers the variation in FF from CTM (panel). The cell strings are partially parallel linked to keep the normal parameters of a 1 m × 1.6 m panel with half-cells or quarter-cells within the range of a full-size 60-cell panel so that the overall current is twice that of the half-cells and the panel voltage is 60× that of a single cell [125]. Because it does not increase edge recombination losses, cutting cells does not affect V_{oc} . In addition to enhancing output at conventional current and voltage levels, the partial parallel connection blocks have a slight effect on sensitivity to partial shading [125]. Inhomogeneous photocurrents in PV cells are caused by shadows on a panel. The serial connectivity forces the actual current for cells in the loop to be the same. Detour diodes bypass the current flowing across a covered string while restricting the system's power output. The parallel connection of cells forces the voltage to be the same; yet, the volume of illumination has little effect on the output voltage. A combination of serial and parallel connections is used to compensate for inhomogeneous irradiance. It is caused by shadowing or soiling. Bifacial panels with half-cells are less susceptible to the unevenness of the rear-side irradiation. It is accomplished by fusing serial and parallel connections. Each substring is made up of 60 cut cells [126] that are joined in a row. The substrings create two parallel strings when cells are divided in half and three parallel strings when cells are divided in thirds [126], [127].

The shingled interconnection panel, which is similar to slate roof shingles, is where the PV cells partially overlap. It produces a high-packing-volume PV panel and is done with both monofacial and bifacial PV cells [128], [129], [130]. *Sun Power* is one of the manufacturers producing commercial shingled panels. Shingled PV panels are made up of PV cells that have been sliced into tiny stripes along the busbars. One cell strip's

p-busbar connects to the other's n-busbar, forming a shingled pattern. The shingled panels are made from monofacial cells. Like monofacial cells, bifacial cells are paired to form a shingled bifacial PV panel. Bifacial cells, as opposed to monofacial cells, use shingled connections. Front and rear metallization grids, cell overlap, number of cell stripes, as well as strong connections that form a panel are optimized for the shingled bifacial panel [131], [132].

To account for a change in rear illumination in bifacial electrical models, a mismatch function based on relative standard deviations in irradiance G must be constructed [133]. The irradiance of a PV cell in a string is determined as it varies according to position and effective self-shading. The accumulation of irradiances is used to compute the relative standard deviation concerning the mismatch loss function. The ratio of P_{string} (maximum power of a string for inhomogeneous irradiance) and the sum of P_{cell} gives the mismatch F_m . When the technique is repeated across several illumination ranges, a trend line for mismatch loss forms. The trend line is used to calculate the mismatch function F_m for each circumstance with a given irradiance (G). A more complex way is to use an electronic circuit simulator in the modeling software for each time step. For bifacial panels, the electrical configuration alters since the location of the connection box is the most noticeable variation. Typically, the series resistance of a bifacial PV panel takes into account the impact of the electrical structure, cross connectors, and linkage to the junction box or boxes [134], [135].

D. Thermal Behavior Modeling of Bifacial Schemes

The electrical behavior of bifacial PV panels responds directly to small and major fluctuations in irradiance. The temperature of the PV cells takes significantly longer to achieve thermal equilibrium with the constantly changing environment. To accurately simulate or forecast the actual temperature of operation for bifacial PV panels, a comprehensive dataset with adequate small-time steps containing ambient temperature, irradiance, wind speed, and direction is required [136]. The temperature of the bifacial panel is affected by the varied optical materials used in comparison to monofacial panels. Around 10% of the surface of the bifacial panel is transparent, indicating that light enters the substrate instead of being reflected or consumed by the back sheet [137]. By thermalizing excited electrons or other processes such as free carrier absorption, photons do not elevate the temperature of the panel over the ambient temperature [137]. The increased power production caused by rear-side incident light suggests that the PV cells are heating up because of thermalization and free carrier absorption. Higher photogenerated current and resistive losses in cells, as well as cell-to-cell connections, contribute to increased power production. They are proportional to the current, and the heat generated by an increase of resistive losses. Building-integrated and building-adapted panels have much greater working temperatures than panels installed on open frames, such as typical monofacial panels on sloped roofs. Bifacial panels are installed in the field on open frames; free-flowing air cools the panel more than panels installed on a sloped roof. The qualities of glass

and polymer back panels differ in terms of heat conductivity, emissivity, and heat transmission to air [138], [139].

E. Testing Standards for Bifacial Panels

The International Electrotechnical Commission's (IEC) technical committee (TC) oversees PV certification programs. Experts in the IEC-appointed TC committees are actively examining current rules and identifying the need for new regulations embracing bifacial PV technology, especially on PV panel standards [140], [141], [142] and technical parts of PV systems [143], [144], [145]. Table III lists the IEC standards according to themes that are critical for standardizing bifacial PV scheme testing. Despite significant contributions from IEC committees, standardizing bifacial PV requires years. IEC frequently introduces helpful techniques in response to specific market demands.

Precise assessment procedures are developed to evaluate the PV energy production of bifacial PV panels, taking into account their ability to generate energy from both the front and back surfaces, and such standards are outlined in *IEC TS 60904-1-2* [143]. The standard defines methodologies for evaluating bifacial power output in daylight or using PV simulator tools, widely used in the PV industry for assessing cell and panel efficacy. Three primary phases are critical in using PV simulators to characterize the generated power of bifacial PV panels: calculating rear-irradiance, induced power increase yield (*BiFi*), and power output under 100 W/m² as well as 200 W/m² rear irradiances.

The comparative efficiency of the rear side of bifacial panels is represented by bifaciality factors, which are described as three ratios in *IEC TS 60904-1-2* [143]. These ratios are derived at STC conditions of 1000 W/m² irradiance, 25 °C, and an air mass of 1.5. If the spectral responses on the front as well as back sides differ, a spectral mismatch correction according to *IEC 60904-7* [146] should be used. The ratio of rear to front-side maximum power is characterized as $\varphi_{p\max}$ and is a crucial relation for bifaciality factor standards determination. The $\varphi_{p\max}$ values for n-PERT bifacial modules range from 75% to 95%, for p-type PERC bifacial panels from 60% to 70%, and for heterojunction technology bifacial panels from >90%. The technique of determining the bifaciality factor at STC is depicted in Fig. 11. A nonreflective clear background ensures a maximum of 3 W/m² at any place on the PV device's nonilluminated surface.

The maximum output power (P_{\max}) is determined utilizing a front irradiance of $G_f = 1000 \text{ W/m}^2$ and numerous rear irradiance (G_r) levels. The G_r values must cover at least two of the following ranges in (5), which represent the vast majority of common rear-side irradiances encountered during field operations [143], [146]

$$G_{ri(i=1,2,3,\dots)} = \begin{cases} 0 < G_{ri} < 100 \text{ W/m}^2 \\ x \leq G_{ri} < 200 \text{ W/m}^2 \\ G_{ri} \geq 200 \text{ W/m}^2 \end{cases} . \quad (5)$$

Based on the applicable PV model, the current TS IEC 60904-1-2 [143] provides two options for achieving single and double-side illumination. The single-side illumination approach facilitates the assessment of the maximum power output (P_{\max}) employing a comparable irradiance $G(E)$ for PV models with

TABLE I
DIFFERENT BIFACIAL PV CELL PARAMETERS

Cell concept	Bi-faciality factor	Si –base	Junction and <i>BSF</i> method for doping	Contacts	Front potential efficiency
Heterojunction [67]	92%	<i>n</i> – type	<i>a</i> – <i>Si</i> : <i>H p</i> – type and <i>n</i> – type	TCO/ <i>Ag</i>	22% – 25%
TOPCon [68]	85%	<i>n</i> – type	Boron–phosphorus diffusion	<i>Ag, Ag/Al</i>	21% – 25%
n-PERT [69]	90%	<i>n</i> – type	Boron–phosphorus diffusion	TCO/ <i>Cu</i>	21% – 22%
p-PERT [70]	90%	<i>p</i> – type	Phosphorus–boron diffusion	<i>Ag, Ag/Al</i>	21% – 22%
PERC+ [71]	80%	<i>p</i> – type	Phosphorus diffusion, local <i>Al</i> – <i>BSF</i>	<i>Ag, Al</i>	21% – 22%
IBC [1]	70%	<i>n</i> – type	Boron–phosphorus diffusion	<i>Ag, Ag/Al</i>	22% – 23%

TABLE II
EFFICIENCIES OF INDUSTRIAL PERC+ PV CELL

Ref.	Year	Efficiency% (Front/Rear)	Organization	Comments
[93]	2021	21.5/16.7	ISFH	No rear <i>Ag</i> pads
[36]	2021	20.3/not published	Trina Solar	Optimized for optical performance in <i>BIPV</i>
[94]	2022	20.7/13.9	Big Sun Energy Technology Inc.	-
[95]	2023	21.5/16.1	Jinko Solar	-
[96]	2023	21.4/not published	Neo Solar Power	-
[97]	2023	21.6/17.3	LONGi Solar	-
[98]	2017	21.6/not published	ISFH	The rear side is optimized for mono-facial use.
[99]	2018	22.1/not published	ISFH	Busbar, <i>Ag</i> front grid design

TABLE III
PV PANEL STANDARDS RELATING TO IEC

Ref.	Theme	Standards of IEC	Modifications for bifacial
[143], [144]	Calibration issues, particularly in estimating electrical power	IEC 60891, IEC60904-X	IEC TS 60904-1-2
[140]	Device compliance evaluation	IEC 61215-X, IEC 61730	Under progress
[142], [145], [147]	PV components and materials	IEC 62852, IEC, 62790, IEC 62930	No changes proposed to date
[141]	Energy Classification	IEC 61853-X	Under progress

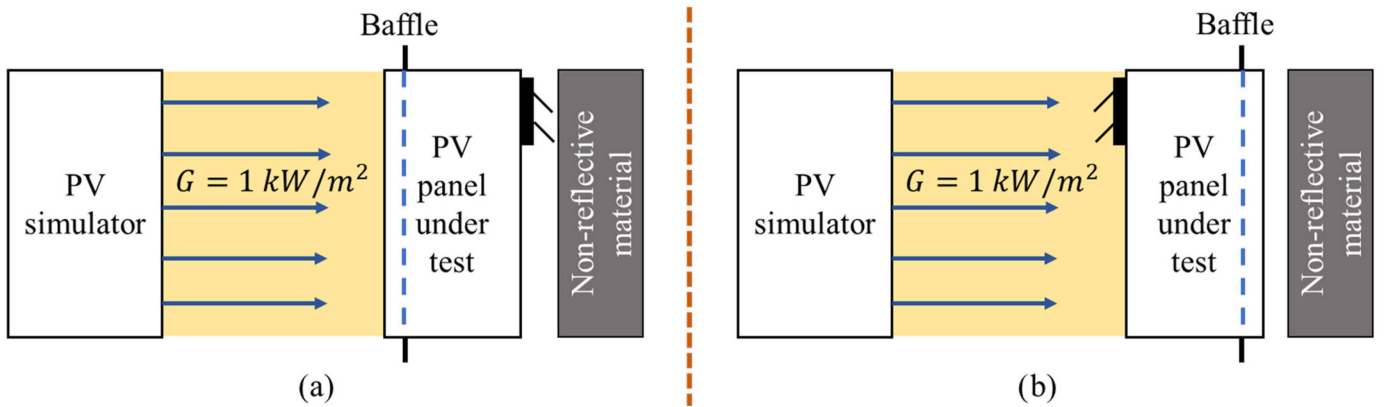


Fig. 11. *IEC TS 60904-1-2* test method for *I*–*V* measurement of bifacial PV modules characterization. (a) Front side. (b) Backside.

just one illumination source, as defined in IEC 60904-9 [148]

$$G(E) = 1000 \frac{W}{m^2} + (\varphi \times G_{ri}) \quad (6)$$

$$\varphi = \text{Min}(\varphi_{I_{sc}}, \varphi_{P_{max}}). \quad (7)$$

The double-sided lighting strategy was created for a PV model with two light sources and adjustable irradiance levels. It is possible to illuminate the front side with $G_f = 1000 \text{ W/m}^2$ and the backside with at least two irradiance levels in the above ranges. Irrespective of the strategy, a P_{max} versus G_r map is essential and G_r is calculated using (6) for the $G(E)$ approach or

assessed for the double-side illumination method. The estimated value of data points is driven to cross the *Y*-axis at P_{max} STC. The slope of such a graph is represented by *BiFi*, which stands for bifacial power gain. The *BiFi* slope is used with the assumption that interpolation can anticipate the device's efficiency based on the front STC and rear irradiance.

Clients are hindered by a lack of exact nominal power specifications for bifacial PV panels. The majority of manufacturers base the power rating on the front side's commonly used STC output power, with others assuming a contribution from the back. There are no clear standards for bifacial PV panel-rated output power nor are there any criteria for how the bifacial

TABLE IV
ELECTRICAL DATA: AN EXAMPLE LABEL FOR A BIFACIAL PV PANEL RATED AT STC AND BSTC (PROPOSED BY *TÜV RHEINLAND*)

Category	STC	BSTC
Nominal power	300 W ($\pm 3\%$)	330 W ($\pm 3.5\%$)
Open-circuit voltage (V_{oc})	38.5 V ($\pm 1\%$)	39 V ($\pm 1.2\%$)
Short-circuit current (I_{sc})	9.4 A ($\pm 2.8\%$)	10.2 A ($\pm 3\%$)
Bi-faciality (φ)	0.7 (± 0.05)	
Maximum system voltage	1000 V IEC	
Maximum OC protection rating	20 A	
Power Temp. coef. (P_{mpp})	-0.4% ($\pm 0.05\%$)	
Voltage Temp. coef. (V_{oc})	-0.31% ($\pm 0.02\%$)	
Current Temp. coef. (I_{sc})	-0.05% ($\pm 0.01\%$)	

attributes should be incorporated on the PV panel's sign or in the company's specification. The IEC is looking into adequate rated output power criteria to provide consistency in the labeling procedure for bifacial PV panels. *TÜV Rheinland* has proposed specific bifacial STCs with front-side irradiances of 1000 W/m^2 and rear-side irradiances of 135 W/m^2 [149]. The National Renewable Energy Laboratory (NREL) [150] and Sandia National Laboratories [151] developed the rear-side irradiance definition, which is related to the following conditions: albedo factor of 0.21, clearance height of 1 m, inclination angle of 37° , and front-side irradiance of 1000 W/m^2 . The optimum power rating of the bifacial panel at bifacial standard testing conditions (BSTCs) is later established to have a standard irradiance of $G(E) = 1000 \text{ W/m}^2 + \varphi \times 135 \text{ W/m}^2$. The IEC firmly considers the BSTC as a criterion for power rating. Table IV [152] depicts an example label for bifacial PV panels with BSTC power characterization [152].

Two criteria are used to assess the quality of PV panel products: module design qualification testing (MQT) according to the IEC 61215 series [140] and module (panel) safety qualification testing (MST) according to the IEC 61730 series [140]. Additional certification requirements for bifacial PV panels are mostly owing to the higher operating electrical currents of these panels. Table V examines the potential additional standards for bifacial PV panels. In 2018, *TÜV Rheinland* presented a unique test technique 2PfG 2665/06.18 [152] to meet the additional certification testing standards for bifacial PV panels. Greater test currents (I_{mpp} or I_{sc} , depending on testing) must be approximated at an equivalent irradiance ($G(E) = 1000 \text{ W/m}^2 + 300 \text{ W/m}^2$) or the $G(E)$ must be used where necessary. However, the STC testing is still used to determine pass/fail requirements (1000 W/m^2 on both front and rear sides) depicted in Fig. 11.

The IEC 61853 guideline set [141] provides a suitable framework for calculating the energy of monofacial PV modules installed in an open rack. The PV industry understands the significance of expanding the energy rating to include developing technologies such as bifacial. On the other hand, the methodology, assessment processes, and associated variability are debated. The advanced PV energy rating (PV-Enerate) European EMPIR project investigated the feasibility of expanding the IEC 61853 guideline sequence to include bifacial devices [141] and Table VI highlights the findings.

V. BIFACIAL PV SYSTEMS

Bifacial PV produces excess yield energy compared with monofacials because of the panel's two-sided light sensitivity. The uncertainty surrounding the actual output of anticipated systems limits potential investment [161], [162]. The approved classification criteria are the measurement of nominal power under standardized conditions (STCs) via a monofacial panel for optimization of a bifacial panel. With simulation tools, predicting the system's energy output with appropriate accuracy is rather simple for monofacials. This is not the case with bifacial devices and systems. When compared with monofacial devices, uncertainty is created by intricate situations. The advantage of bifaciality is related to the intensity of light on the panel's back-side. It is determined by ground reflectivity, seasonal weather, light homogeneity, and the system size; smaller bifacial systems tend to have higher backside rear irradiance than large bifacial systems (the edge effect on the rear irradiance). Shade effects at the backside of the PV device and the reflecting ground are unavoidable for free-standing panels. The multiple-panel system includes features such as direct shading by neighboring row panels or indirect shading by surrounding panels. As a result, the rear-side irradiation is lowered. Analyzing power plant energy output is a method of determining the efficiency of precise installations. Furthermore, data from larger systems are uncommon because of installation and shadowing conditions [163].

$$G_{\text{bifacial}} = \frac{E_{\text{bifacial}} - E_{\text{monofacial}}}{E_{\text{monofacial}}} \times 100\%. \quad (8)$$

Here, G_{bifacial} denotes the bifacial gain. $E_{\text{monofacial}}$ and E_{bifacial} are the specific yield (kWh/kWp) of monofacial and bifacial PV panels under identical conditions. The bifacial gain is used to represent the benefit of bifaciality. It refers to the difference in energy yield between bifacial and monofacial devices with identical installation conditions. The kWh/kWp ratio is typically examined. The STCs front-side measurement of the bifacial panel is reflected in the kWp data. Because of the lack of consideration over the influence of shading factors on bifacial output, a comparison of measurement data from different systems reveals significant variation. The higher energy yield is the attraction of bifacial PV. Monofacial panels are ineffective for several applications. In this regard, the vertical mounting of PV systems in an E-W configuration is the most widely discussed. It is very beneficial in snowy areas and desert locations [164]. It helps to ensure continuous energy production throughout the day, which improves the alignment of electricity production and demand.

In the case of vertical E/W systems, factors become more intricate, and there are fewer sources of information available. In these cases, the panel type and albedo are significant, but so is the mounting configuration of the reference panel and the installation latitude. When compared with a vertically installed monofacial panel, a bifacial gain of more than 100% (Table VII) is observed.

Besides, a comparison with a slanted south-oriented monofacial panel is more intriguing. In high latitudes, where the amount

TABLE V
SAFETY AND QUALITY CONFIGURATION OF BIFACIAL PV PANEL

Test	Practice for Mono-facial PV	Bi-facial testing issues
Thermal cycling test (<i>MQT 11/MST 51</i>) [153]	The experiment was carried out in an atmospheric setting with constant temperature fluctuations ranging from -40 to $+85^{\circ}\text{C}$. To further stress the soldering joints, a current equal to I_{mpp} is introduced.	The maximum possible current must account for the influence from the backside.
Bypass-diode test (<i>MQT 18/MST 25</i>) [154]	For the first hour, the current being applied is $-I_{\text{sc}}$, and for the second hour, it is $-1.25 \times I_{\text{sc}}$.	The heating effects are amplified when the current input from the backside is incorporated.
Hot-spot endurance test (<i>MQT 09/MST 22</i>) [155]	The power loss at just one shaded cell is set to the maximum allowable, which is defined by the panel's maximum electrical current (I_{mpp}).	The maximum power current must account for the influence from the rear.
Temperature test (<i>MST 21</i>) [155]	The element and material benchmark temperatures correspond to a 1000 W/m^2 front irradiation and a 40°C room temperature.	The higher the rear-side irradiance of bi-facial PV panels, the higher the temperatures.
Reverse current overload test (<i>MST 26</i>) [132]	This test guarantees that inverse currents generated during outdoor exercise will not cause panel problems because of welding joint heating. The test current is $1.35 \times$ the maximum reverse current specified on the panel supplier's nameplate.	The maximum reverse current should correspond to the most extreme outdoor scenario, such as 1300 W/m^2 front-side irradiance with a high albedo and sun tracking.

TABLE VI
PV ENERATE EXTENSION OF THE IEC 61853 STANDARD SERIES TO BIFACIAL PV PANELS

Ref.	Aspect	Monofacial PV	Bifacial PV
[156]	Scenarios of mounting	With a 20° inclination angle and towards the equator	Add an east–west (E–W) rack with a low albedo.
[157]	Irradiance from the rear	Not available	Hourly data for rear-side irradiance were gathered for a medium/high albedo (Equator facing at 20°); the data were considered homogenous.
[158], [159]	Factor of spectral correction	Exclusively at the front	The spectral response at the panel's back and the spectral albedo beneath the panel have been revised.
[160]	Profiles of climate	For the front side	Angle of inclination for the new planes (E–W and inclination plane's backside), spectral irradiance, beam, and diffuse on the inclined plane's back-side

TABLE VII
BIFACIAL GAINS FOR VARIOUS N-PERT PANEL PLACEMENT SCHEME

Ref.	Geometry of bi-facial installation and latitude	Mono-facial reference installation geometry	Albedo	Bi-facial gain
[165]	<i>San Felipe, Chile</i> (32°S) has a slanted fixed tilt	Fixed tilt (slanted)	65%–75%	30%
[166]	Vertical installation in the <i>United States</i>	Vertical	Not measured	100%
[167]	<i>Winterthur, Switzerland</i> (47°N) vertical installation	Slanted fixed tilt	25%	10%
[168]	Vertical installation at <i>Saar</i> (49°N), <i>Germany</i>	Slanted fixed tilt	25%	10%
[169], [170]	Vertical installation in <i>El Gouna</i> (27°N) <i>Egypt</i>	Slanted fixed tilt	25%	–5%
[171]	In <i>La Silla, Chile</i> (29°S), a single axis was tracked	Single-axis tracked	25%	15%

of scattered sunlight is greater and the vertical mounting is closer to the optimal tilted angle, an electrical gain of 10% is obtained, whereas an electrical loss of 5% was found in low latitudes [180], [181], [182]. This application is still appealing for a variety of reasons, including minimal ground coverage, a higher generating peak, and fewer soiling issues with vertical installations. Table VII lists numerous setups and the accompanying bifacial gains for n-PERT panels. *MegaCell* [183] and *Enel* [184] employ typical monofacial panels with white backsheets as a foundation for comparison in large bifacial systems in Chile and observed that the experimental bifacial advantages differ slightly. Several incidences with varying albedo in the case of the fixed-tilt S/N panel system have already been observed across the world. Depending on the substrate albedo (25% for raw sand and 75% [185] for white stones), bifacial improvements of 15% to 30% are attainable.

Fig. 12(a) [59] shows the development of PV panels for special markets and regional applications. Based on regional environments, the development of specialized panels for a specific

market is required; however, the modifications are not that significant. The modifications are mostly based on bifacial panels compared with monofacial ones [186], [187]. Fig. 12(b) [59] and Table VIII depict the various specific PV system implications for the next two decades and the fundamental factors of floating and agri-PV, respectively. It can be observed that although water bodies are abundant compared with land, agri-PV will be a dominant endues PV system for the next decade compared with floating PV [59] because of the agri-PV system's maintenance and initial installation cost being much lower than floating PV systems. The agri-PV and floating PV systems are effective when bifacial PV panels are used instead of monofacial PV panels. It is because, in these unique PV end-use systems, vertical panel installation is an effective option. Since bifacial panels respond to solar irradiation on each surface of the panel, therefore, in these unique PV end-use systems, bifacial panels are more effective than monofacial ones.

Bifacial systems based on single-axis tracking have attracted greater attention in recent years since experimental results in

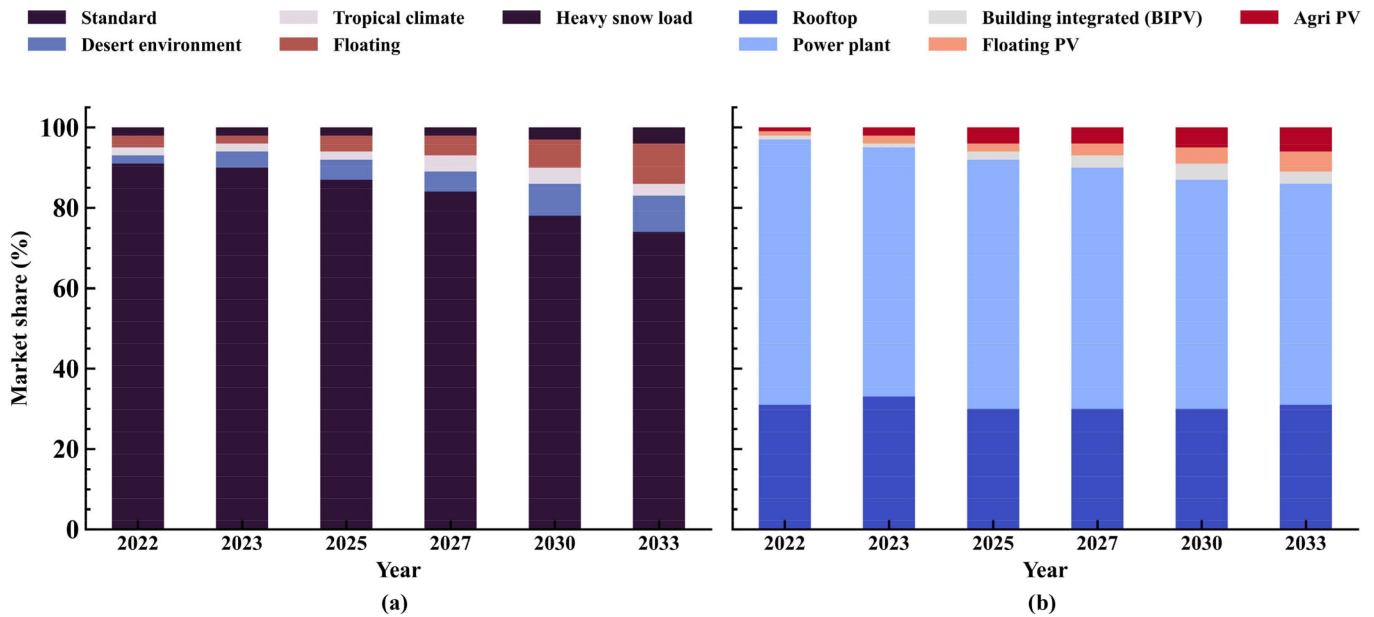


Fig. 12. ITRPV technology share projection. (a) Regional application. (b) Different PV end-use system.

TABLE VIII
FUNDAMENTAL FACTORS BETWEEN GROUND-MOUNTED AND FLOATING BIFACIAL PV SCHEME

Ref.	Theme	Ground installed PV	Floating PV
[172], [173]	Structure for PV module support	Steel-based racking structure	Floats constructed primarily of high-density polyethylene
[174]	Wiring	Standard	Waterproof and marine-grade materials
[173], [174]	Stability	Pile pushed with a concrete foundation	Mooring lines are used for bank or bottom anchoring.
[175]	Preparation of the site	Geotechnical investigation, soil leveling, and grading	Bathymetry study, hydrodynamic survey, and geotechnical investigation
[174]	Factors of external loading	Wind and snow	Wind, snow, waves, water currents, water depth, and variation in water level
[176]	Tilt Angle	33°	10°
[177]	Levelized operation and maintainers (\$/kW - yr)	18	15.5
[178]	IP (ingress protection) Rating	Lower than IP66	Greater than IP67
[179]	Sales tax, shipping and handling, and a contingency fund	5%, 0%, 3%	5%, 5%, 5%
[177], [179]	Overhead for the developer, EPC (engineering procurement construction) overhead, and net profit	7.7%, 10.9%, 7.84%	7.7%, 10.9%, 7.84%

large systems demonstrated that the bifacial gain in those conditions is likewise extremely important. Numerous tracking mount solutions are near optimal for bifacial panels since they are located high above the ground and have a wide row distance. As a result, the bifacial gains show advantages over monofacial single-axis tracking and are quite comparable to fixed-tilt systems. This was initially reported by *Enel in la Silla* [171]. Combining single-axis tracking with bifacial panels leads to electrical benefits of more than 40% over fixed-tilt monofacial panels in systems with high albedo [188].

A. Vertically Planted Bifacial PV System

Bifacial systems with a south orientation are appealing for installation schemes that would be impossible with standard monofacial systems. An attractive alternative is a vertical installation with an east/west orientation. It is a promising application

strategy [181], [189], [190]. The installation design avoids the largest power-generating peak at noon. As a result, the generation profile becomes diverse [182], [191]. New concepts include broadening the generating profile and reducing dust deposition or snow load with the use of simulation data and measurements on single, vertically placed modules [12], [13]. Vertically placed systems experience significant shadowing, and the energy generation is strongly dependent on the precise layout of the PV installation [192], [193]. The bifacial panels are dual-purpose gadgets. One example is functional for buildings such as noise barriers. The other are the subjects of scientific investigation into the behavior of vertical bifacial systems. Bifacial panels have become more affordable in recent years as demand has increased and manufacturing capacity has expanded [192]. The vertical installation concept has gained popularity and is now employed in utility-scale ground-mounted systems.

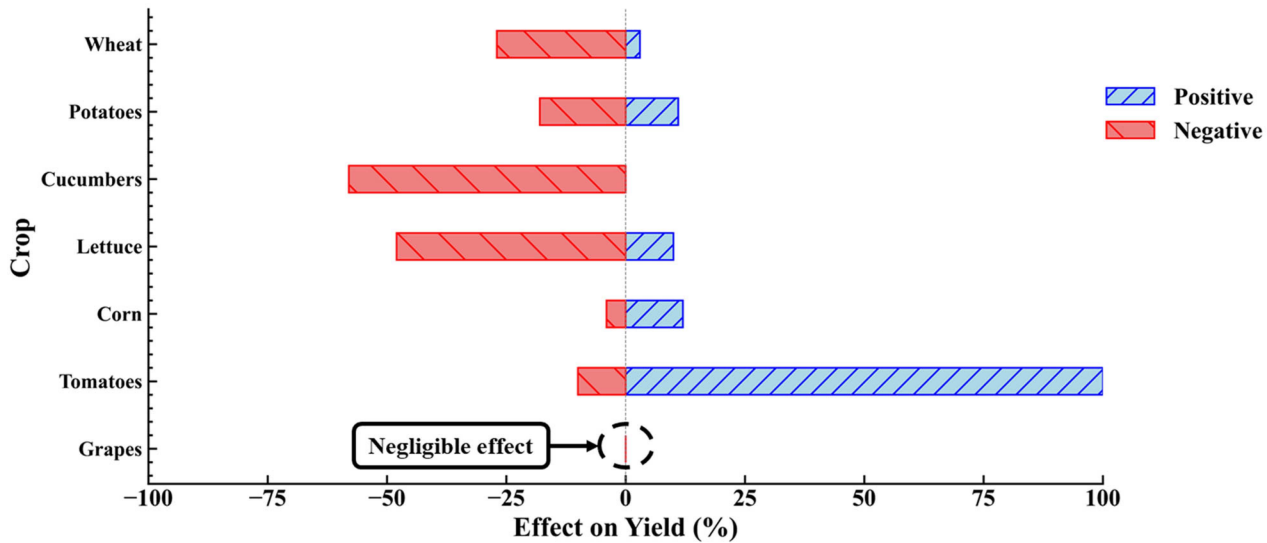


Fig. 13. Crop yield impact for agri-bifacial PV across numerous landscapes.

B. Agri-Photovoltaics System With Bifacial

Agri-PV is the combination of farming and PV within the same area of land. The elevated installation of PV panels at a height of 4 m [194] from the ground is a popular solution for agri-PV. It allows agricultural machinery to drive through and utilize the area below [194], [195]. The shadows on the ground are caused by the panel array. It might be advantageous or disadvantageous depending on the environment and crops to be grown. Vertical bifacial PV plants are an innovative approach to agri-PVs. There is no ground coverage or effect on irradiation dispersion or rainfall for vertical E/W installation. The row pitch of these installations is 10–20 m [196]. It allows conventional agricultural machinery to use newer GPS-controlled machines [196].

Fig. 13 illustrates a variety of cultivars with yield variations dependent on location and environment [197], [198], [199], [200], [201], [202], [203]. The selection of plant species and cultivars for vegetative, grazing, as well as crop production, is crucial to the success of an agri-PV venture. The purpose of InSPIRE [204] research and other research programs is to establish which plants and cultivars are best suited to specific places that are significantly influenced by geographical environment and water-soil quality. Vegetation selection is frequently included in a larger framework of locally influenced choices, such as the owner's preference for native species or local ecotypes. Types that thrive in partial shade are occasionally surprising; for example, researchers were surprised when "sun-loving" kinds of grass outnumbered "shade-loving" grass types in research testing patches at an ecosystem service InSPIRE study location in Colorado [205]. Furthermore, as revealed by InSPIRE research in Western Oregon, different cultivars of the same plants, such as potatoes, act dramatically differently under identical conditions [206]. Crop rotation is critical over numerous years because crops such as nightshade affect soil conditions. Crop vegetation success is measured yearly for agricultural goods

and five years after the first planting for vegetation/ecosystem projects.

Table IX lists the agri-PV with bifacial applications such as crop and food production, livestock production, ecosystem service provision through vegetation management, and PV greenhouses [207], [208], [209]. These uses are not mutually exclusive, and various activities can take place on the same site at the same time or even in the same area of the location at various times of year. Numerous projects have distinct zones for agricultural production or ecosystem service production, while others use the same zones for diverse reasons, such as targeted grazing in pollinator habitat zones for tactical vegetation control at certain times of the year. The limited shade of PV architecture has an impact on crop production systems; crops are planted precisely beneath panels and in between rows of panels. Crop management is done by hand or with mechanical equipment.

Crop production takes place within a standard ground-mounted PV installation, or the infrastructure is altered in terms of panel height, panel spacing, row spacing, or other design elements to accommodate changes in sunlight/shading patterns and compatibility with agricultural activities [208]. Innovative methods and configurations are being investigated to support types of crops and horticulture, such as orchards, vineyards, field crops, and other fruits [209]. Agri-PV systems for livestock and animal husbandry include grazing and animal management beneath, around, and directly adjacent to PV equipment. Practitioners have generally used sheep, cattle, poultry, honeybees, and rabbits to implement agri-PV systems, although other animal activities are also conceivable [168], [207], [209]. Depending on the demands of the PV site and the animal management, animals can be on-site year-round, seasonally, or on an as-needed basis. Animals do not get all of their nutrition from on-site resources, and they are required to be moved regularly or supplemented with nutrients from offsite sources. The connectivity of PV infrastructure with aquaculture activities is a

TABLE IX
COMMERCIALLY DEPLOYED TYPES OF AGRI-BIFACIAL PV SCHEMES

Traditional utility scheme (fixed-tilt-slanted)	Alternate scheme	Comment	Bi-facial gain
Crop production	Vertical, tracker stilt mount	Crop grown in between rows	100% (vertical), [166] and 10% (Tracker stilt mount), [167]
Animal husbandry Ecosystem services	Elevated reinforced panels Greenhouse PV	Grazing in between and underneath panels Vegetation grown in between and underneath panels	15%, [171] 30%, [165]

growing use, although not all countries consider it an agri-PV category. Traditional utility-scale PV facilities do not need to be significantly altered in many cases to accommodate cattle grazing and veterinary activities; however, other site design changes such as vegetation planting and management, fencing, water supply, and animal access are included to ensure integration with animal husbandry practices. Agri-PVs for vertical bifacial systems have a lack of experience. Practical consequences are necessary to evaluate the feasibility of dual use of land farms with PV agriculture.

C. Floating-PV System With Bifacial

Water as the foundation for bifacial PV is a new application field. The land use of ground-mounted bifacial PV systems is the cause for floating PV with bifacial panels. Land for large-scale PV is scarce, and it competes for agricultural use. There is insufficient acreage to supply renewable energy on a local scale. Given that water covers 71% of the earth's surface area, it appears sensible to explore floating PV with bifacial. Large patches of freshwater are available, while the water surface's function is not jeopardized. Energy generation and alternative water usage can occur concurrently. Commercial and agricultural irrigation reservoirs, gravel and sand extraction excavations, water bodies, and canals are some examples. Aside from freshwater uses, the seas and oceans have enormous surface area potential. Several systems and companies are attempting to construct at-sea autonomous PV power plant projects [210], [211]. The enormous scale of projects is a significant advantage of floating PV with bifacial schemes. Many water regions are vastly larger than available land areas, resulting in higher project scales and cheaper cost per kilowatt. The floating PV including the bifacial panel schemes system is more expensive than ground-mounted systems in terms of initial cost. Larger project scales and water benefits are predicted to result in a lower overall leveled cost of power for water-based systems over a duration of a larger period [212], [213].

D. Single-Axis Tracked Bifacial PV System

Horizontal single-axis tracking has become a significant technology in maximizing energy yield in places near the equator. It is to minimize the electricity generation concerning the leveled cost of electricity. The bifaciality, combined with tracking, was thought not to be compatible. It is because of the contractor's belief that aggregating mechanical structures economically degrades the system's LCOE. Nevertheless, tracking with bifacial panels makes sense and leads to high power generation.

Horizontal single-axis tracking became popular in large PV system installations [3], [16], [214], [215], [216]. Barros E Silva et al. [217] presented simulation research comparing the properties and productivity of monofacial and bifacial PV panels as well as compared the employment of trackers in the creation of horizontal modules. Russell et al. [218] proposed DUET—a bifacial PV performance model that calculates optical and electrical performance based on a physically representative array geometry and incorporates single-axis tracking. Sreenath et al. [219] investigated the performance of conceptual bifacial PV systems under varied albedo conditions while taking a tracking system into account and considered a white-colored surface area of the BIPV system. Kalhoro et al. [220] created a system that mimics the bifacial paradigm and includes an economic benefit for developing countries having considered single-axis tracking.

VI. LEVELIZED COST OF ELECTRICITY FOR BIFACIAL PV SYSTEMS

The cost of electricity generated by bifacial PV systems is an important consideration. It compares the efficiency of PV to that of traditional alternative energy sources. From an economic standpoint, it is an electricity-producing mechanism that discusses PV panel technology and how to configure a system for a certain use and territory. Research and development (R&D) initiatives in the PV manufacturing value chain aim to reduce the cost of bifacial PV-generated electricity. It begins with the purification of Si feedstock and finishes with the design and installation of PV systems. In terms of components, operation, and maintenance, the LCOE is a statistic that attempts to encompass all costs associated with the building and operation of a PV system, as well as all factors influencing total electricity output (kWh) over the lifetime of the PV system.

$$\text{LCOE} = \frac{\text{Total life cycle cost}}{\text{Total life time electricity generation}}. \quad (9)$$

Calculation of the LCOE of a specific project using (9) necessitates the use of information such as taxes, credits, and feed-in-tariffs. The system advisor model (SAM) was developed by the NREL, Sandia National Laboratory, and the United States Department of Energy, and it includes a freely accessible LCOE estimation application that allows for the selection of different economic models as well as the execution of the critical economic factors [221]. A thorough definition of the LCOE idea considers funding conditions as well as the fact that money spent in the future has a lesser value than money spent today. The latter is a key notion in financial mathematics and is implemented by the "net present value" concept. The

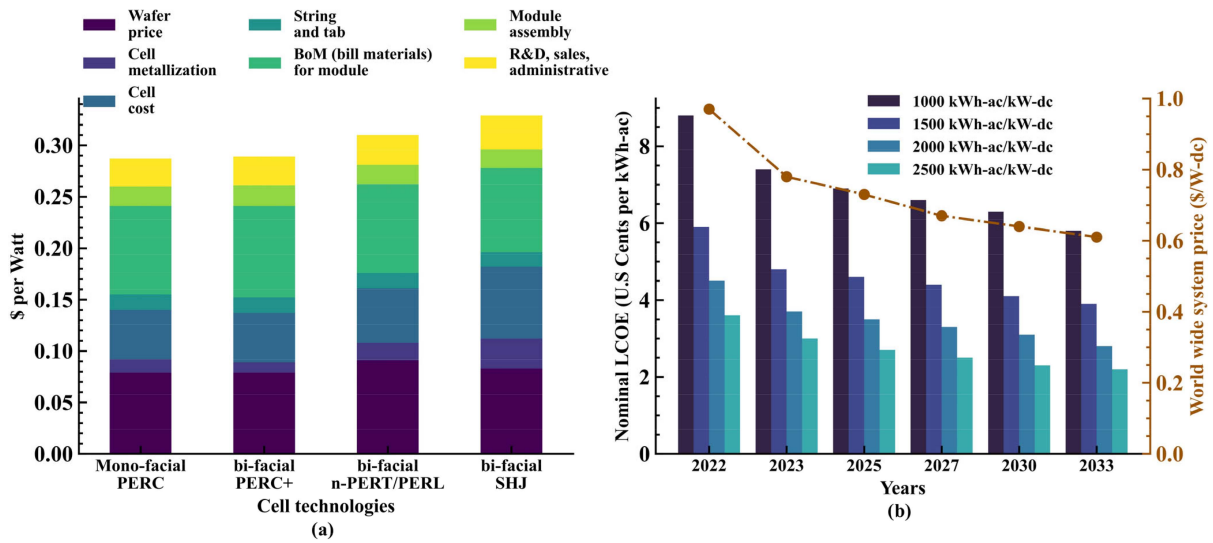


Fig. 14. (a) Module (panel) cost comparison for mono- and bifacial PVs. (b) Global LCOE for various insolation scenarios and capital costs: 2023 ITRPV survey.

LCOE is defined as the energy price (\$/kWh) at which the whole project cost's net present value is zero. The LCOE is the averaged levelized energy price (\$/kWh) across the project's entire lifecycle at which the project achieves a financial break [221].

$$\text{LCOE} = \sum_{t=1}^N \frac{(I_t + O_t)(1+d)^t}{E_t/(1+d)^t}. \quad (10)$$

Equation (10) is the detailed version of (9), where I_t is the repayment-debt and equity in year t and O_t is the expenses-operation as well as maintenance for year t . E_t and d are energy produced (kWh) in a year as well as the discount rate, respectively [222]. The initial energy yield kWh/kWp is used to compute the energy generation. It is determined by the location of the plant's design and the panel technology used. The total electricity generation for the first year of operation is calculated by multiplying the initial energy yield by the nominal plant capacity (Wp at STCs). To calculate the energy generation for each year of the power plant's lifetime, a yearly degradation rate of performance of the bifacial PV system is considered [223].

Fig. 14(a) compares the panel cost for monofacial and bifacial cell technologies based on the database of the NREL [150] PV panel production cost statistics. It shows that the R&D phase has a higher dollar per watt rate for bifacial compared with monofacial showing that bifacial technologies R&D investments are on the rise. However, the remaining aspects in terms of higher energy yield and panel dimension are relatively more cost effective for bifacial modules than monofacial ones. For PERC cells, the module assembly process contributes to the higher cost of bifacial PV modules. For n-PERT/PERL cells, the costs associated with Si-wafer and cell processing are the most significant aspects. Fig. 14(b) depicts the global LCOE for different insolation using the 2023 ITRPV [59] system survey, the predictions were performed using NREL's [150] SAM cash flow structure [221]. The LCOE predictions are applied for both mono- and bifacial PV systems. The predictions show that the

LCOE for bifacial PV systems is expected to have optimum conditions in the next decade.

VII. FUTURE OF BIFACIAL PV

In the SNECS in Shanghai 2022 and Intersolar Europe in South America 2022 conferences, the presentation topics were comprised of bifacial panels [224], [225]. The vision of the main PV businesses was promoted. They presented high-efficiency, low-cost n-type bifacial technology. The devices used carrier-selective connections, which resulted in efficiencies of more than 25%, similar to what SunPower and Panasonic have been doing for years. The sole distinction is that the costs must be comparable to those of ordinary PV cells [226]. As predicted by ITRPV [59], more than 40% of the panels on the market are based on fundamental bifacial technologies. According to Bloomberg [227], PV is the most critical energy source. PV volume and cost projections have historically been understated. This is true for the Bloomberg study's 100 GWp market. PV's influence on bifaciality is more than projected, with a 100 GWp market share in less than five years [227], [228], [229].

VIII. CONCLUSION

A comparative study of the monofacial and the bifacial technologies has been carried out, as reported in the literature. The current status and prospects of both cell technologies are discussed. Findings suggest that bifacial c-Si TOPCon, and SHJ cell technologies show high cell efficiency as well as bifaciality factor while having optimum fabrication techniques compared with alternate cell technologies. Study shows that electrical-optical-thermal modeling of bifacial PV panels is necessary to optimize bifacial cell efficiency, which also helps to minimize bifacial cell-to-panel loss. The bifacial PV panel's dual use of land cases, such as vertical bifacial, agri-PV with bifacial, and floating-PV with bifacial panels, gives a clear advantage over monofacial ones. Findings show that for the next few decades, agri-PV will surpass floating-PV with bifacial because of minimum maintenance and initial installation costs. The LCOE

(levelized cost of electricity) is a crucial evaluation metric for bifacial PV systems for the assessment of financial benefit over monofacial PV systems. It was found that in the next decade, the LCOE of the mono- and bifacial PV system's capital cost will drop by 40%, as claimed by recent ITRPV reports. Findings suggest that the bifaciality factor and bifacial gain provide the direct differentiating factor compared with monofacial PV systems.

Various Si cell technologies are rapidly adopting bifacial layout in the world market share of cell fabrication. In recent years, the cell fabrication to module layout cost comparison of mono- and bifacial PVs shows that the latter is cost-effective in terms of optimum energy yield and module/panel dimension.

ACKNOWLEDGMENT

The authors would like to thank Brac University for providing support toward this study.

REFERENCES

- [1] R. Kopecek et al., "ZEBRA technology: Low cost bifacial IBC solar cells in mass production with efficiency exceeding 23.5%," in *Proc. Conf. Rec. IEEE Photovolt. Spec. Conf.*, 2020, pp. 1008–1012, doi: [10.1109/PVSC45281.2020.9300503](https://doi.org/10.1109/PVSC45281.2020.9300503).
- [2] C. Zhang et al., "Bifacial p-type PERC solar cell with efficiency over 22% using laser doped selective emitter," *Energies*, vol. 13, no. 6, Mar. 2020, Art. no. 1388, doi: [10.3390/EN13061388](https://doi.org/10.3390/EN13061388).
- [3] T. M. Mahim et al., "Experimental evaluation of the performance: A novel bi-facial PV panel," in *Proc. IEEE Region 10 Symp.*, 2023, pp. 1–6, doi: [10.1109/TENSYMP55890.2023.10223485](https://doi.org/10.1109/TENSYMP55890.2023.10223485).
- [4] A. A. Abdallah et al., "Thermal behavior and photovoltaic performance of monofacial and bifacial silicon heterojunction modules under desert conditions," in *Proc. Conf. Rec. IEEE Photovolt. Spec. Conf.*, 2021, pp. 843–845, doi: [10.1109/PVSC43889.2021.9518402](https://doi.org/10.1109/PVSC43889.2021.9518402).
- [5] C. Han et al., "Towards bifacial silicon heterojunction solar cells with reduced TCO use," *Prog. Photovolt., Res. Appl.*, vol. 30, no. 7, pp. 750–762, Jul. 2022, doi: [10.1002/PIP.3550](https://doi.org/10.1002/PIP.3550).
- [6] T. Dullweber and J. Schmidt, "Industrial silicon solar cells applying the passivated emitter and rear cell (PERC) concept-A review," *IEEE J. Photovolt.*, vol. 6, no. 5, pp. 1366–1381, Sep. 2016, doi: [10.1109/JPHOTOVOL.2016.2571627](https://doi.org/10.1109/JPHOTOVOL.2016.2571627).
- [7] S. Singh et al., "Large area co-plated bifacial n-PERT cells with polysilicon passivating contacts on both sides," *Prog. Photovolt., Res. Appl.*, vol. 30, no. 8, pp. 899–909, Aug. 2022, doi: [10.1002/PIP.3548](https://doi.org/10.1002/PIP.3548).
- [8] J. G. Kang, J. H. Kim, and J. T. Kim, "Design elements and electrical performance of a bifacial BIPV module," *Int. J. Photoenergy*, vol. 2016, 2016, Art. no. 6943936, doi: [10.1155/2016/6943936](https://doi.org/10.1155/2016/6943936).
- [9] W. Gu, T. Ma, M. Li, L. Shen, and Y. Zhang, "A coupled optical-electrical-thermal model of the bifacial photovoltaic module," *Appl. Energy*, vol. 258, Jan. 2020, Art. no. 114075, doi: [10.1016/J.APENERGY.2019.114075](https://doi.org/10.1016/J.APENERGY.2019.114075).
- [10] Q. Bai et al., "Investigation on bifaciality factor and ideality factor of PERC bifacial solar module under different irradiances," in *Proc. Conf. Rec. IEEE Photovolt. Spec. Conf.*, 2021, pp. 248–251, doi: [10.1109/PVSC43889.2021.9518575](https://doi.org/10.1109/PVSC43889.2021.9518575).
- [11] L. Kreinin et al., "PV module power gain due to bifacial design: Preliminary experimental and simulation data," in *Proc. Conf. Rec. IEEE Photovolt. Spec. Conf.*, 2010, pp. 2171–2175, doi: [10.1109/PVSC2010.5615874](https://doi.org/10.1109/PVSC2010.5615874).
- [12] M. H. Riaz, H. Imran, R. Younas, and N. Z. Butt, "The optimization of vertical bifacial photovoltaic farms for efficient agrovoltaic systems," *Sol. Energy*, vol. 230, pp. 1004–1012, Dec. 2021, doi: [10.1016/J.SOLENER.2021.10.051](https://doi.org/10.1016/J.SOLENER.2021.10.051).
- [13] T. Baumann et al., "Photovoltaic systems with vertically mounted bifacial PV modules in combination with green roofs," *Sol. Energy*, vol. 190, pp. 139–146, Sep. 2019, doi: [10.1016/J.SOLENER.2019.08.014](https://doi.org/10.1016/J.SOLENER.2019.08.014).
- [14] S. G. Gulhane and A. R. Phadke, "Design of Agro-photovoltaic system for optimized energy generation and crop yield using Fuzzy Framework," in *Proc. 2nd Int. Conf. Innov. Technol.*, 2023, pp. 1–6, doi: [10.1109/IN-OCON57975.2023.10101340](https://doi.org/10.1109/IN-OCON57975.2023.10101340).
- [15] A. A. Widayat, S. Ma'arif, K. D. Syahindra, A. F. Fauzi, and E. A. Setiawan, "Comparison and optimization of floating bifacial and monofacial solar PV system in a tropical region," in *Proc. 9th Int. Conf. Power Sci. Eng.*, 2020, pp. 66–70, doi: [10.1109/ICPSE51196.2020.9354374](https://doi.org/10.1109/ICPSE51196.2020.9354374).
- [16] D. Berrian, J. Libal, M. Klenk, H. Nussbaumer, and R. Kopecek, "Performance of bifacial PV arrays with fixed tilt and horizontal single-axis tracking: Comparison of simulated and measured data," *IEEE J. Photovolt.*, vol. 9, no. 6, pp. 1583–1589, Nov. 2019, doi: [10.1109/JPHOTOVOLTO.2019.2924394](https://doi.org/10.1109/JPHOTOVOLTO.2019.2924394).
- [17] M. T. Patel et al., "When and where to track: A worldwide comparison of single-axis tracking vs. fixed tilt bifacial farms," in *Proc. Conf. Rec. IEEE Photovolt. Spec. Conf.*, 2020, pp. 1735–1737, doi: [10.1109/PVSC45281.2020.9300692](https://doi.org/10.1109/PVSC45281.2020.9300692).
- [18] M. A. Green, "Third generation photovoltaics: Assessment of progress over the last decade," in *Proc. Conf. Rec. IEEE Photovolt. Spec. Conf.*, 2009, pp. 146–149, doi: [10.1109/PVSC.2009.5411708](https://doi.org/10.1109/PVSC.2009.5411708).
- [19] G. Conibeer, "Third-generation photovoltaics," *Mater. Today*, vol. 10, no. 11, pp. 42–50, Nov. 2007, doi: [10.1016/S1369-7021\(07\)70278-X](https://doi.org/10.1016/S1369-7021(07)70278-X).
- [20] M. A. Green, K. Emery, Y. Hishikawa, and W. Warta, "Solar cell efficiency tables (version 33)," *Prog. Photovolt., Res. Appl.*, vol. 17, no. 1, pp. 85–94, Jan. 2009, doi: [10.1002/PIP.880](https://doi.org/10.1002/PIP.880).
- [21] A. Mulazzani, P. Eleftheriadis, and S. Leva, "Recycling c-Si PV modules: A review, a proposed energy model and a manufacturing comparison," *Energies*, vol. 15, no. 22, Nov. 2022, Art. no. 8419, doi: [10.3390/EN15228419](https://doi.org/10.3390/EN15228419).
- [22] K. E. Knapp and R. R. Gay, "Research on high-efficiency, large-area, CuInSe₂ based thin-film modules," *rheI*, Jan. 1994, [Online]. Available: <https://ui.adsabs.harvard.edu/abs/1994rheI.rept....K>
- [23] "China: World's largest energy consumer; surpasses the U.S. - IER." [Online]. Available: <https://www.instituteforenergyresearch.org/fossil-fuels/coal/china-worlds-largest-energy-consumer-surpasses-the-u-s/>
- [24] S. W. Glunz, R. Preu, and D. Biro, "Crystalline silicon solar cells: State-of-the-art and future developments," in *Comprehensive Renewable Energy*, Amsterdam, The Netherlands: Elsevier, Jan. 2012, pp. 353–387, doi: [10.1016/B978-0-08-087872-0-00117-7](https://doi.org/10.1016/B978-0-08-087872-0-00117-7).
- [25] S. W. Glunz and R. Preu, "Crystalline silicon solar cells – State-of-the-art and future developments," in *Comprehensive Renewable Energy*, 2nd ed. Amsterdam, The Netherlands: Elsevier, vol. 1/9, Jan. 2022, vol. 1, pp. 293–324, doi: [10.1016/B978-0-12-819727-1-00129-1](https://doi.org/10.1016/B978-0-12-819727-1-00129-1).
- [26] G. M. Wilson et al., "The 2020 photovoltaic technologies roadmap," *J. Phys. D, Appl. Phys.*, vol. 53, no. 49, Sep. 2020, Art. no. 493001, doi: [10.1088/1361-6463/AB9C6A](https://doi.org/10.1088/1361-6463/AB9C6A).
- [27] N. Song, S. Deng, N. Song, and S. Deng, "Thin film deposition technologies and application in photovoltaics," in *Thin Films - Deposition Methods and Applications*. London, U.K.: IntechOpen, Nov. 2022, doi: [10.5772/INTECHOPEN.108026](https://doi.org/10.5772/INTECHOPEN.108026).
- [28] N. Balaji et al., "Review on metallization in crystalline silicon solar cells," in *Solar Cells*. London, U.K.: IntechOpen, Jul. 2019, doi: [10.5772/INTECHOPEN.84820](https://doi.org/10.5772/INTECHOPEN.84820).
- [29] O. O. Abegunde et al., "Overview of thin film deposition techniques," *AIMS Mater. Sci.*, vol. 6, no. 2, pp. 174–199, 2019, doi: [10.3934/MATER-SCI.2019.2.174](https://doi.org/10.3934/MATER-SCI.2019.2.174).
- [30] "Table comparison: Physical vapor deposition vs. Chemical vapor deposition." [Online]. Available: <https://www.sputtertargets.net/blog/table-comparison-physical-and-chemical-vapor-deposition.html>
- [31] T. Gao et al., "An industrially viable TOPCon structure with both ultra-thin SiO_x and n+-poly-Si processed by PECVD for p-type c-Si solar cells," *Sol. Energy Mater. Sol. Cells*, vol. 200, Nov. 21, 2023, Art. no. 109926.
- [32] B. van de Loo et al., "On the hydrogenation of poly-Si passivating contacts by Al₂O₃ and SiN_x thin films," *Sol. Energy Mater. Sol. Cells*, vol. 215, Nov. 21, 2023, Art. no. 110592.
- [33] Y. Chen et al., "25% large-area industrial silicon solar cell: Learning from history and future perspective," in *Proc. 36th Eur. Photovolt. Sol. Energy Conf. Exhib.*, 2019, pp. 1–6.
- [34] D. Chen et al., "24.58% total area efficiency of screen-printed, large area industrial silicon solar cells with the tunnel oxide passivated contacts (i-TOPCon) design," *Sol. Energy Mater. Sol. Cells*, vol. 206, Nov. 21, 2023, Art. no. 110258.

- [35] E. Lohmuller et al., "Towards 90% bifaciality for p-type cz-Si solar cells by adaption of industrial PERC processes," in *Proc. IEEE 7th World Conf. Photovolt. Energy Convers., Joint Conf. 45th IEEE PVSC, 28th PVSEC 34th EU PVSEC*, 2018, pp. 3727–3731, doi: [10.1109/PVSC.2018.8548202](https://doi.org/10.1109/PVSC.2018.8548202).
- [36] J. Yu et al., "Improved bifacial properties of P-type passivated emitter and rear cell solar cells toward high mass production efficiency," *Physica Status Solidi*, vol. 218, no. 14, Jul. 2021, Art. no. 2100059, doi: [10.1002/PSSA.202100059](https://doi.org/10.1002/PSSA.202100059).
- [37] R. Islam and K. C. Saraswat, "Metal/insulator/semiconductor carrier selective contacts for photovoltaic cells," in *Proc. IEEE 40th Photovolt. Spec. Conf.*, 2014, pp. 285–289, doi: [10.1109/PVSC.2014.6924915](https://doi.org/10.1109/PVSC.2014.6924915).
- [38] S. Singh et al., "Development of 2-sided polysilicon passivating contacts for co-plated bifacial n-PERT cells," in *Proc. Conf. Rec. IEEE Photovolt. Spec. Conf.*, 2020, pp. 449–452, doi: [10.1109/PVSC45281.2020.9300834](https://doi.org/10.1109/PVSC45281.2020.9300834).
- [39] D. Ding, G. Lu, Z. Li, Y. Zhang, and W. Shen, "High-efficiency n-type silicon PERT bifacial solar cells with selective emitters and poly-Si based passivating contacts," *Sol. Energy*, vol. 193, pp. 494–501, Nov. 2019, doi: [10.1016/J.SOLENER.2019.09.085](https://doi.org/10.1016/J.SOLENER.2019.09.085).
- [40] S. Cao et al., "Stable MoOX-based heterocontacts for p-type crystalline silicon solar cells achieving 20% efficiency," *Adv. Funct. Mater.*, vol. 30, no. 49, Dec. 2020, Art. no. 2004367, doi: [10.1002/ADFM.202004367](https://doi.org/10.1002/ADFM.202004367).
- [41] M. H. Saw, Y. S. Khoo, J. P. Singh, and Y. Wang, "Enhancing optical performance of bifacial PV modules," *Energy Procedia*, vol. 124, pp. 484–494, 2017, doi: [10.1016/J.EGYPRO.2017.09.285](https://doi.org/10.1016/J.EGYPRO.2017.09.285).
- [42] J. A. M. van Roosmalen et al., "White bifacial modules - improved STC performance combined with bifacial energy yield," in *Proc. ECN*, 2016.
- [43] J. Kim et al., "Scalable high-efficiency bi-facial solar evaporator with a dendritic copper oxide wick," *ACS Appl. Mater. Interfaces*, vol. 13, no. 10, pp. 11869–11878, Mar. 2021, doi: [10.1021/AC-SAMI.0C21570/SUPPL_FILE/AM0C21570_SI_003.MP4](https://doi.org/10.1021/AC-SAMI.0C21570/SUPPL_FILE/AM0C21570_SI_003.MP4).
- [44] J. R. Sharma, G. Das, A. B. Roy, S. Bose, and S. Mukhopadhyay, "Design analysis of heterojunction solar cells with aligned AZO nanorods embedded in p-type Si wafer," *Silicon*, vol. 12, no. 2, pp. 305–316, Feb. 2020, doi: [10.1007/S12633-019-00134-4/METRICS](https://doi.org/10.1007/S12633-019-00134-4/METRICS).
- [45] O. Volovlikova, S. Gavrilov, and P. Lazarenko, "Influence of illumination on porous silicon formed by photo-assisted etching of p-type Si with a different doping level," *Micromachines*, vol. 11, no. 2, Feb. 2020, Art. no. 199, doi: [10.3390/MI11020199](https://doi.org/10.3390/MI11020199).
- [46] J. Zhao, C. Qin, J. Guo, and H. Wei, "Iterative correction of the thickness for transmission-mode GaAs photocathode optical performance," *Optik (Stuttgart)*, vol. 175, pp. 334–339, Dec. 2018, doi: [10.1016/J.OPTIK.2018.09.036](https://doi.org/10.1016/J.OPTIK.2018.09.036).
- [47] M. Kopytko, K. Jóźwikowski, P. Martyniuk, and A. Rogalski, "Photon recycling effect in small pixel p-i-n HgCdTe long wavelength infrared photodiodes," *Infrared Phys. Technol.*, vol. 97, pp. 38–42, Mar. 2019, doi: [10.1016/J.INFRARED.2018.12.015](https://doi.org/10.1016/J.INFRARED.2018.12.015).
- [48] J. Yu et al., "Simulation of the influence of absorber thickness and doping concentration on non-equilibrium photovoltaic long-wavelength HgCdTe infrared detectors," *J. Electron. Mater.*, vol. 52, no. 7, pp. 4801–4808, Jul. 2023, doi: [10.1007/S11664-023-10391-0](https://doi.org/10.1007/S11664-023-10391-0).
- [49] C. Ghennai, F. F. Ahmad, O. Rejeb, and A. K. Hamid, "Sensitivity analysis of design parameters and power gain correlations of bi-facial solar PV system using response surface methodology," *Sol. Energy*, vol. 223, pp. 44–53, Jul. 2021, doi: [10.1016/J.SOLENER.2021.05.024](https://doi.org/10.1016/J.SOLENER.2021.05.024).
- [50] L. Yunqiao and F. Yan, "An innovative power prediction method for bifacial PV modules," *Electr. Eng.*, vol. 105, pp. 2151–2159, Aug. 2023, doi: [10.1007/S00202-023-01805-7](https://doi.org/10.1007/S00202-023-01805-7).
- [51] S. Touré, "Effect of the dynamic resistance on the maximum output power in dynamic modelling of photovoltaic solar cells," *Open J. Model. Simul.*, vol. 10, no. 1, pp. 48–57, 2022, doi: [10.4236/OJMSI.2022.101003](https://doi.org/10.4236/OJMSI.2022.101003).
- [52] T. C. R. Russell, R. Saive, A. Augusto, S. G. Bowden, and H. A. Atwater, "The influence of spectral albedo on bifacial solar cells: A theoretical and experimental study," *IEEE J. Photovolt.*, vol. 7, no. 6, pp. 1611–1618, Nov. 2017, doi: [10.1109/JPHOTOV.2017.2756068](https://doi.org/10.1109/JPHOTOV.2017.2756068).
- [53] G. Raina and S. Sinha, "A simulation study to evaluate and compare monofacial vs bifacial PERC PV cells and the effect of albedo on bifacial performance," *Mater. Today Proc.*, vol. 46, pp. 5242–5247, Jan. 2021, doi: [10.1016/J.MATPR.2020.08.632](https://doi.org/10.1016/J.MATPR.2020.08.632).
- [54] A. Cuevas, A. Luque, J. Eguren, and J. del Alamo, "50 percent more output power from an albedo-collecting flat panel using bi-facial solar cells," *Sol. Energy*, vol. 29, no. 5, pp. 419–420, 1982, doi: [10.1016/0038-092X\(82\)90078-0](https://doi.org/10.1016/0038-092X(82)90078-0).
- [55] A. Diao, B. Thiaw, M. Boiro, S. Mbodji, and G. Sissoko, "A junction electric field determination of a bifacial silicon solar cell under a constant magnetic field effect by using the photoconductivity method," *J. Mod. Phys.*, vol. 12, no. 5, pp. 635–645, 2021, doi: [10.4236/JMP.2021.125041](https://doi.org/10.4236/JMP.2021.125041).
- [56] M. A. Green, "The passivated emitter and rear cell (PERC): From conception to mass production," *Sol. Energy Mater. Sol. Cells*, vol. 143, pp. 190–197, Dec. 2015, doi: [10.1016/J.SOLMAT.2015.06.055](https://doi.org/10.1016/J.SOLMAT.2015.06.055).
- [57] D. Xu et al., "Illumination-induced hole doping for performance improvement of graphene/n-silicon solar cells with P3HT interlayer," *Adv. Electron. Mater.*, vol. 3, no. 3, Mar. 2017, Art. no. 1600516, doi: [10.1002/AELM.201600516](https://doi.org/10.1002/AELM.201600516).
- [58] L. J. Geerligs and D. Macdonald, "Base doping and recombination activity of impurities in crystalline silicon solar cells," *Prog. Photovolt., Res. Appl.*, vol. 12, no. 4, pp. 309–316, Jun. 2004, doi: [10.1002/PIP.546](https://doi.org/10.1002/PIP.546).
- [59] "International Technology Roadmap for Photovoltaic (ITRPV) - vdma.Org - VDMA," [Online]. Available: <https://www.vdma.org/international-technology-roadmap-photovoltaic>
- [60] R. Kopecek et al., "Bifaciality: One small step for technology, one giant leap for kWh cost reduction," *Photovolt. Int.*, vol. 26, pp. 32–45, 2015.
- [61] I. Shoukry, J. Libal, R. Kopecek, E. Wefringhaus, and J. Werner, "Modelling of bifacial gain for stand-alone and in-field installed bifacial PV modules," *Energy Procedia*, vol. 92, pp. 600–608, Aug. 2016, doi: [10.1016/J.EGYPRO.2016.07.025](https://doi.org/10.1016/J.EGYPRO.2016.07.025).
- [62] J. Raban-Alarbach and A. Schneider, "Anti-reflective coated glass and its impact on bifacial modules' temperature in desert locations," *Energy Procedia*, vol. 92, pp. 590–599, Aug. 2016, doi: [10.1016/j.egypro.2016.07.024](https://doi.org/10.1016/j.egypro.2016.07.024).
- [63] E. Molin, B. Stridh, A. Molin, and E. Wackelgard, "Experimental yield study of bifacial PV modules in nordic conditions," *IEEE J. Photovolt.*, vol. 8, no. 6, pp. 1457–1463, Nov. 2018, doi: [10.1109/JPHOTOV.2018.2865168](https://doi.org/10.1109/JPHOTOV.2018.2865168).
- [64] D. Chen et al., "An efficient TeO₂/Ag transparent top electrode for 20%-efficiency bifacial perovskite solar cells with a bifaciality factor exceeding 80%," *J. Mater. Chem. A Mater.*, vol. 7, no. 25, pp. 15156–15163, Jun. 2019, doi: [10.1039/C9TA02389E](https://doi.org/10.1039/C9TA02389E).
- [65] I. Cesar et al., "Efficiency gain for bi-facial multi-crystalline solar cell with uncapped Al₂O₃ and local firing-through Al-BSF," in *Proc. Conf. Rec. IEEE Photovolt. Spec. Conf.*, 2013, pp. 1212–1217, doi: [10.1109/PVSC.2013.6744358](https://doi.org/10.1109/PVSC.2013.6744358).
- [66] A. Moehlecke, I. Zanesco, A. P. Mallmann, D. Eberhardt, and G. F. Pereira, "MetalizaÇÃ serigráfica de células solares bifaciais," in *XI Congresso Brasileiro de Energia*, vol. 2, pp. 945–955, 2006.
- [67] W. Long et al., "On the limiting efficiency for silicon heterojunction solar cells," *Sol. Energy Mater. Sol. Cells*, vol. 231, Oct. 2021, Art. no. 111291, doi: [10.1016/J.SOLMAT.2021.111291](https://doi.org/10.1016/J.SOLMAT.2021.111291).
- [68] Q. Wang et al., "High-efficiency n-TOPCon bifacial solar cells with selective poly-Si based passivating contacts," *Sol. Energy Mater. Sol. Cells*, vol. 259, Aug. 2023, Art. no. 112458, doi: [10.1016/J.SOLMAT.2023.112458](https://doi.org/10.1016/J.SOLMAT.2023.112458).
- [69] Z. W. Peng, T. Buck, L. J. Koduvvelikulathu, V. D. Mihaileti, and R. Kopecek, "Industrial screen-printed n-PERT-RJ solar cells: Efficiencies beyond 22% and open-circuit voltages approaching 700 mV," *IEEE J. Photovolt.*, vol. 9, no. 5, pp. 1166–1174, Sep. 2019, doi: [10.1109/JPHOTOV.2019.2919117](https://doi.org/10.1109/JPHOTOV.2019.2919117).
- [70] J. Fichtner, G. Micard, F. Koschnick, H. Zunft, A. Zuschlag, and G. Hahn, "APCVD based stacked co-diffusion for multicrystalline silicon p-PERT solar cells," in *Proc. 36th Eur. Photovolt. Sol. Energy Conf. Exhib.*, 2019, pp. 161–166.
- [71] K. Sporleder et al., "Potential-induced degradation of bifacial PERC solar cells under illumination," *IEEE J. Photovolt.*, vol. 9, no. 6, pp. 1522–1525, Nov. 2019, doi: [10.1109/JPHOTOV.2019.2937231](https://doi.org/10.1109/JPHOTOV.2019.2937231).
- [72] L. E. Black and D. H. Macdonald, "On the quantification of Auger recombination in crystalline silicon," *Sol. Energy Mater. Sol. Cells*, vol. 234, Jan. 2022, Art. no. 111428, doi: [10.1016/J.SOLMAT.2021.111428](https://doi.org/10.1016/J.SOLMAT.2021.111428).
- [73] D. Lachenal et al., "Optimization of tunnel-junction IBC solar cells based on a series resistance model," *Sol. Energy Mater. Sol. Cells*, vol. 200, Sep. 2019, Art. no. 110036, doi: [10.1016/J.SOLMAT.2019.110036](https://doi.org/10.1016/J.SOLMAT.2019.110036).
- [74] S. H. Yoo and H. J. Choi, "Solar architecture integrated bi-facial photovoltaic system as a shade," *Processes*, vol. 9, no. 9, Sep. 2021, Art. no. 1625, doi: [10.3390/PR9091625](https://doi.org/10.3390/PR9091625).
- [75] A. S. A. Ahmed et al., "MoS₂ZIF-8 derived nitrogen doped carbon (NC)-PEDOT: PSS as optically transparent counter electrode for dye-sensitized solar cells," *Sol. Energy*, vol. 218, pp. 117–128, Apr. 2021, doi: [10.1016/J.SOLENER.2021.02.032](https://doi.org/10.1016/J.SOLENER.2021.02.032).

- [76] A. Ottana et al., "Outdoor energy performances for standard and bi-facial modules as well on the failure modes observed in Outdoor conditions," in *Proc. Conf. Rec. IEEE Photovolt. Spec. Conf.*, 2022, pp. 554–556, doi: [10.1109/PVSC48317.2022.9938501](https://doi.org/10.1109/PVSC48317.2022.9938501).
- [77] Y. Liu et al., "High-efficiency silicon heterojunction solar cells: Materials, devices and applications," *Mater. Sci. Eng. R, Rep.*, vol. 142, Oct. 2020, Art. no. 100579, doi: [10.1016/J.MSER.2020.100579](https://doi.org/10.1016/J.MSER.2020.100579).
- [78] N. El-Atab, S. F. Shaikh, S. M. Khan, and M. M. Hussain, "Bi-facial substrates enabled heterogeneous multi-dimensional integrated circuits (MD-IC) for Internet of things (IoT) applications," *Adv. Eng. Mater.*, vol. 21, no. 7, Jul. 2019, Art. no. 1900043, doi: [10.1002/ADEM.201900043](https://doi.org/10.1002/ADEM.201900043).
- [79] Y. Chen et al., "Mass production of industrial tunnel oxide passivated contacts (i-TOPCon) silicon solar cells with average efficiency over 23% and modules over 345 W," *Prog. Photovolt., Res. Appl.*, vol. 27, no. 10, pp. 827–834, Oct. 2019, doi: [10.1002/PIP.3180](https://doi.org/10.1002/PIP.3180).
- [80] "TOPCon – Overcoming fundamental bottlenecks to a new world-record silicon solar cell - Fraunhofer ISE." [Online]. Available: <https://www.ise.fraunhofer.de/en/research-projects/topcon.html>
- [81] Q. Wang et al., "High-efficiency n-TOPCon bifacial solar cells with selective poly-Si based passivating contacts," *Sol. Energy Mater. Sol. Cells*, vol. 259, Aug. 2023, Art. no. 112458, doi: [10.1016/J.SOLMAT.2023.112458](https://doi.org/10.1016/J.SOLMAT.2023.112458).
- [82] C. Sen et al., "Accelerated damp-heat testing at the cell-level of bifacial silicon HJT, PERC and TOPCon solar cells using sodium chloride," *Sol. Energy Mater. Sol. Cells*, vol. 262, Oct. 2023, Art. no. 112554, doi: [10.1016/J.SOLMAT.2023.112554](https://doi.org/10.1016/J.SOLMAT.2023.112554).
- [83] S. Simayi, Y. Kida, K. Shirasawa, T. Suzuki, and H. Takato, "Method of removing single-side doped layer while maintaining pyramid textured surface of n-type bifacial solar cells," *IEEE J. Photovolt.*, vol. 7, no. 2, pp. 458–462, Mar. 2017, doi: [10.1109/JPHOTOV.2016.2646060](https://doi.org/10.1109/JPHOTOV.2016.2646060).
- [84] K. Nakamura, T. Kawatsu, T. Kamioka, and Y. Ohshita, "Performance improvement of front junction n-type PERT solar cell by wafer thinning," in *Proc. IEEE 7th World Conf. Photovolt. Energy Convers., Joint Conf. 45th IEEE PVSC, 28th PVSEC 34th EU PVSEC*, 2018, pp. 1536–1539, doi: [10.1109/PVSC.2018.854785](https://doi.org/10.1109/PVSC.2018.854785).
- [85] W. Luo et al., "Investigation of potential-induced degradation in n-PERT bifacial silicon photovoltaic modules with a glass/glass structure," *IEEE J. Photovolt.*, vol. 8, no. 1, pp. 16–22, Jan. 2018, doi: [10.1109/JPHOTOV.2017.2762587](https://doi.org/10.1109/JPHOTOV.2017.2762587).
- [86] L. Kreinin, N. Bordin, N. Eisenberg, P. Grabitz, and G. Wahl, "Industrially fabricated bifacial Si solar cells with n+-p-p+ structure," in *Proc. 28th Eur. Photovolt. Sol. Energy Conf.*, vol. 30, 2013.
- [87] J. Fichtner, H. Zunft, A. Zuschlag, H. Knauss, and G. Hahn, "Getting efficacy of APCVD-based process steps for low-cost PERT-type multicrystalline silicon solar cells," *IEEE J. Photovolt.*, vol. 8, no. 6, pp. 1464–1469, Nov. 2018, doi: [10.1109/JPHOTOV.2018.2865509](https://doi.org/10.1109/JPHOTOV.2018.2865509).
- [88] T. Dullweber et al., "PERC+: Industrial PERC solar cells with rear Al grid enabling bifaciality and reduced Al paste consumption," *Prog. Photovolt., Res. Appl.*, vol. 24, no. 12, pp. 1487–1498, Dec. 2016, doi: [10.1002/PIP.2712](https://doi.org/10.1002/PIP.2712).
- [89] "N-type bi-facial solar cells with boron emitters from doped PECVD layers." Accessed: Aug. 22, 2023. [Online]. Available: <https://kops.uni-konstanz.de/entities/publication/7e45b015-0f0e-4a77-9d5f-c761e183c550>
- [90] K. Kim and W. N. Shafarman, "Alternative device structures for CIGS-based solar cells with semi-transparent absorbers," *Nano Energy*, vol. 30, pp. 488–493, Dec. 2016, doi: [10.1016/J.NANOEN.2016.10.038](https://doi.org/10.1016/J.NANOEN.2016.10.038).
- [91] M. Edoff, J. Joel, B. Vermang, and C. Hagglund, "Back contact passivation effects in bi-facial thin CIGS solar cells," in *Proc. Conf. Rec. IEEE Photovolt. Spec. Conf.*, Nov. 2016, vol. 2016, pp. 3527–3530, doi: [10.1109/PVSC.2016.7750326](https://doi.org/10.1109/PVSC.2016.7750326).
- [92] J. Farrell, E. Bastola, M. Jamarkattel, M. Heben, and R. F. Klie, "Characterizing the back-contact interface of bi-facial polycrystalline CdTe devices using transmission electron microscopy," in *Proc. Conf. Rec. IEEE Photovolt. Spec. Conf.*, 2022, pp. 884–886, doi: [10.1109/PVSC48317.2022.9938728](https://doi.org/10.1109/PVSC48317.2022.9938728).
- [93] M. Sall et al., "Back illuminated N/P/P+ bifacial silicon solar cell under modulated short-wavelength: Determination of base optimum thickness," *Energy Power Eng.*, vol. 13, no. 5, pp. 207–220, May 2021, doi: [10.4236/EPE.2021.135014](https://doi.org/10.4236/EPE.2021.135014).
- [94] R. Liu, L. Yin, and Y. Zhou, "An improved process for bifacial n-PERT solar cells fabricated with phosphorus activation and boron diffusion in one-step high temperature," *J. Wuhan Univ. Technol., Mater. Sci. Ed.*, vol. 37, no. 6, pp. 1056–1060, Dec. 2022, doi: [10.1007/S11595-022-2633-9/METRICS](https://doi.org/10.1007/S11595-022-2633-9/METRICS).
- [95] "Jinko Solar-." [Online]. Available: <https://www.jinkosolar.com/en/site/bifacial>
- [96] V. Petrova-Koch, R. Hezel, and A. Goetzberger, *High-Efficient Low-Cost Photovoltaics*. Springer, 2008.
- [97] "LONGi green energy technology Co Ltd Executive & employee information - globaldata." [Online]. Available: <https://www.globaldata.com/company-profile/longi-green-energy-technology-co-ltd/executives/>
- [98] B. Radfar, F. Es, and R. Turan, "Investigation on different surface modifications using laser texturing," in *Proc. 33rd Eur. Photovolt. Sol. Energy Conf. Exhib.*, 2017, pp. 706–709, doi: [10.4229/EU-PVSEC20172017-2AV.2.48](https://doi.org/10.4229/EU-PVSEC20172017-2AV.2.48).
- [99] T. Dullweber et al., "Present status and future perspectives of bifacial PERC+ solar cells and modules," *JaJAP*, vol. 57, no. 8, Aug. 2018, Art. no. 08RA01, doi: [10.7567/JJAP.57.08RA01](https://doi.org/10.7567/JJAP.57.08RA01).
- [100] Y. S. Lim, C. K. Lo, S. Y. Kee, H. T. Ewe, and A. R. Faiz, "Design and evaluation of passive concentrator and reflector systems for bifacial solar panel on a highly cloudy region – A case study in Malaysia," *Renewable Energy*, vol. 63, pp. 415–425, Mar. 2014, doi: [10.1016/J.RENENE.2013.10.008](https://doi.org/10.1016/J.RENENE.2013.10.008).
- [101] G. Razongles et al., "Bifacial photovoltaic modules: Measurement challenges," *Energy Procedia*, vol. 92, pp. 188–198, Aug. 2016, doi: [10.1016/J.EGYPRO.2016.07.056](https://doi.org/10.1016/J.EGYPRO.2016.07.056).
- [102] L. Kreinin, A. Karsenty, D. Grobgeld, and N. Eisenberg, "PV systems based on bifacial modules: Performance simulation vs. design factors," in *Proc. IEEE 44th Photovolt. Spec. Conf.*, 2016, pp. 2688–2691, doi: [10.1109/PVSC.2016.7750138](https://doi.org/10.1109/PVSC.2016.7750138).
- [103] P. Hacke et al., "Development of an IEC test for crystalline silicon modules to qualify their resistance to system voltage stress," *Prog. Photovolt., Res. Appl.*, vol. 22, no. 7, pp. 775–783, Jul. 2014, doi: [10.1002/PIP.2434](https://doi.org/10.1002/PIP.2434).
- [104] D. B. Sulas-Kern et al., "Feasibility and performance analysis of bifacial module under extremely hot and dry climate," *Eng. Res. Exp.*, vol. 5, no. 1, Feb. 2023, Art. no. 015024, doi: [10.1088/2631-8695/ACB1F1](https://doi.org/10.1088/2631-8695/ACB1F1).
- [105] B. P. Song et al., "End-of-life management of bifacial solar panels using high-voltage fragmentation as pretreatment approach," *J. Clean. Prod.*, vol. 276, Dec. 2020, Art. no. 124212, doi: [10.1016/J.JCLEPRO.2020.124212](https://doi.org/10.1016/J.JCLEPRO.2020.124212).
- [106] S. M. Dasari, P. Srivastav, R. Shaw, S. Saravanan, and P. Suratkar, "Optimization of cell to module conversion loss by reducing the resistive losses," *Renewable Energy*, vol. 50, pp. 82–85, Feb. 2013, doi: [10.1016/j.renene.2012.05.022](https://doi.org/10.1016/j.renene.2012.05.022).
- [107] J. Singh, Y. Khoo, J. Chai, Z. Liu, and Y. Wang, "Cell-to-module power loss/gain analysis of silicon wafer-based PV modules," vol. 31, pp. 98–105, 2016.
- [108] I. M. Peters, Y. S. Khoo, and T. M. Walsh, "Detailed current loss analysis for a PV module made with textured multicrystalline silicon wafer solar cells," *IEEE J. Photovolt.*, vol. 4, no. 2, pp. 585–593, Mar. 2014, doi: [10.1109/JPHOTOV.2013.2295736](https://doi.org/10.1109/JPHOTOV.2013.2295736).
- [109] J. P. Singh, A. G. Aberle, and T. M. Walsh, "Electrical characterization method for bifacial photovoltaic modules," *Sol. Energy Mater. Sol. Cells*, vol. 127, pp. 136–142, Aug. 2014, doi: [10.1016/J.SOLMAT.2014.04.017](https://doi.org/10.1016/J.SOLMAT.2014.04.017).
- [110] R. Witteck et al., "Improved STC and energy yield performance of bifacial modules with white-grid rear reflectors," in *Proc. Conf. Rec. IEEE Photovolt. Spec. Conf.*, 2022, vol. 2022, pp. 1245–1247, doi: [10.1109/PVSC48317.2022.9938599](https://doi.org/10.1109/PVSC48317.2022.9938599).
- [111] A. Onno et al., "Predicted power output of silicon-based bifacial tandem photovoltaic systems," *Joule*, vol. 4, no. 3, pp. 580–596, Mar. 2020, doi: [10.1016/J.JOULE.2019.12.017](https://doi.org/10.1016/J.JOULE.2019.12.017).
- [112] J. Manuel Longares, A. García-Jiménez, and N. García-Polanco, "Multiphysics simulation of bifacial photovoltaic modules and software comparison," *Sol. Energy*, vol. 257, pp. 155–163, Jun. 2023, doi: [10.1016/J.SOENER.2023.04.005](https://doi.org/10.1016/J.SOENER.2023.04.005).
- [113] G. Razongles et al., "Bifacial photovoltaic modules: Measurement challenges," *Energy Procedia*, vol. 92, pp. 188–198, Aug. 2016, doi: [10.1016/j.egypro.2016.07.056](https://doi.org/10.1016/j.egypro.2016.07.056).
- [114] M. H. Saw, Y. S. Khoo, J. P. Singh, and Y. Wang, "Enhancing optical performance of bifacial PV modules," *Energy Procedia*, vol. 124, pp. 484–494, Sep. 2017, doi: [10.1016/J.EGYPRO.2017.09.285](https://doi.org/10.1016/J.EGYPRO.2017.09.285).
- [115] M. R. Vogt et al., "PV module current gains due to structured backsheets," *Energy Procedia*, vol. 124, pp. 495–503, 2017, doi: [10.1016/j.egypro.2017.09.286](https://doi.org/10.1016/j.egypro.2017.09.286).
- [116] U. A. Yusufoglu et al., "Simulation of energy production by bifacial modules with revision of ground reflection," *Energy Procedia*, vol. 55, pp. 389–395, Jan. 2014, doi: [10.1016/J.EGYPRO.2014.08.111](https://doi.org/10.1016/J.EGYPRO.2014.08.111).
- [117] M. Basta, Z. Kuznicki, M. Hosatte Marek Basta, Z. T. Kuznicki, and M. Hosatte, "SIM-SEG code giving a complete insight into electronic and photovoltaic performances basing on non-destructive optical measurements," *Proc. Photon. Sol. Energy Syst. IX*, vol. 12150, pp. 62–69, May 2022, doi: [10.1117/12.2622101](https://doi.org/10.1117/12.2622101).

- [118] M. Singh et al., "Comparing optical performance of a wide range of perovskite/silicon tandem architectures under real-world conditions," *Nanophotonics*, vol. 10, no. 8, pp. 2043–2057, Jun. 2021, doi: [10.1515/NANOPH-2020-0643/ASSET/GRAPHIC/J_NANOPH-2020-0643 FIG_010.JPG](https://doi.org/10.1515/NANOPH-2020-0643/ASSET/GRAPHIC/J_NANOPH-2020-0643 FIG_010.JPG).
- [119] A. Julien et al., "Backside light management of 4-terminal bifacial perovskite/silicon tandem PV modules evaluated under realistic conditions," *Opt. Exp.*, vol. 28, no. 25, pp. 37487–37504, Dec. 2020, doi: [10.1364/OE.405713](https://doi.org/10.1364/OE.405713).
- [120] H. P. Yin et al., "Optical enhanced effects on the electrical performance and energy yield of bifacial PV modules," *Sol. Energy*, vol. 217, pp. 245–252, Mar. 2021, doi: [10.1016/J.SOLENER.2021.02.004](https://doi.org/10.1016/J.SOLENER.2021.02.004).
- [121] B. M. Cote, I. M. Slauch, M. G. Deceglie, T. J. Silverman, and V. E. Ferry, "Light management in bifacial photovoltaics with spectrally selective mirrors," *ACS Appl. Energy Mater.*, vol. 4, no. 6, pp. 5397–5402, Jun. 2021, doi: [10.1021/ACSAEM.1C01236/SUPPL_FILE/AE1C01236_SI_001.PDF](https://doi.org/10.1021/ACSAEM.1C01236/SUPPL_FILE/AE1C01236_SI_001.PDF).
- [122] J. Walter, M. Tranitz, M. Volk, C. Ebert, and U. Eitner, "Multi-wire interconnection of busbar-free solar cells," *Energy Procedia*, vol. 55, pp. 380–388, Jan. 2014, doi: [10.1016/J.EGYPRO.2014.08.109](https://doi.org/10.1016/J.EGYPRO.2014.08.109).
- [123] Y. Yao et al., "Module integration of solar cells with diverse metallization schemes enabled by SmartWire Connection Technology," in *Proc. IEEE 42nd Photovolt. Spec. Conf.*, New Orleans, LA, USA, 2015, pp. 1–5, doi: [10.1109/PVSC.2015.7355648](https://doi.org/10.1109/PVSC.2015.7355648).
- [124] A. Schneider, L. Rubin, and G. Rubin, "Solar cell efficiency improvement by new metallization techniques—the day4TM electrode concept," in *Proc. Conf. Rec. IEEE 4th World Conf. Photovolt. Energy Convers.*, 2006, vol. 1, pp. 1095–1098, doi: [10.1109/WCPEC.2006.279333](https://doi.org/10.1109/WCPEC.2006.279333).
- [125] J. Bagdahn, J. Schneider, and H. Hanifi, "Reduced shading effect on half-cell modules—Measurement and simulation," in *Proc. 31th Eur. Photovolt. Sol. Energy Conf. Exhib.*, 2015, pp. 2529–2533, doi: [10.4229/EU-PVSEC20152015-5CV.2.25](https://doi.org/10.4229/EU-PVSEC20152015-5CV.2.25).
- [126] P. Baliozian et al., "Postmetallization ‘passivated edge technology’ for separated silicon solar cells," *IEEE J. Photovolt.*, vol. 10, no. 2, pp. 390–397, Mar. 2020, doi: [10.1109/JPHOTOV.2019.2959946](https://doi.org/10.1109/JPHOTOV.2019.2959946).
- [127] A. Singh and D. Jones, "Snow shedding properties of bifacial PV panels," in *Proc. Conf. Rec. IEEE Photovolt. Spec. Conf.*, 2022, pp. 646–648, doi: [10.1109/PVSC48317.2022.9938947](https://doi.org/10.1109/PVSC48317.2022.9938947).
- [128] Y. Zhang, M. Kim, L. Wang, P. Verlinden, and B. Hallam, "Design considerations for multi-terawatt scale manufacturing of existing and future photovoltaic technologies: Challenges and opportunities related to silver, indium and bismuth consumption," *Energy Environ. Sci.*, vol. 14, no. 11, pp. 5587–5610, Nov. 2021, doi: [10.1039/D1EE01814K](https://doi.org/10.1039/D1EE01814K).
- [129] M. T. Zarmai, N. N. Ekere, C. F. Oduoza, and E. H. Amalu, "A review of interconnection technologies for improved crystalline silicon solar cell photovoltaic module assembly," *Appl. Energy*, vol. 154, pp. 173–182, Sep. 2015, doi: [10.1016/J.APENERGY.2015.04.120](https://doi.org/10.1016/J.APENERGY.2015.04.120).
- [130] M.-J. Park, M. Kim, J. Shin, S.-B. Byeon, and C. Jeong, "Fabrication of shingled design bifacial c-Si photovoltaic modules," *Curr. Photovolt. Res.*, vol. 10, no. 1, pp. 1–5, Mar. 2022, doi: [10.21218/CPR.2022.10.1.001](https://doi.org/10.21218/CPR.2022.10.1.001).
- [131] V. Kanneboina, "Detailed review on c-Si/a-Si:H heterojunction solar cells in perspective of experimental and simulation," *Microelectron. Eng.*, vol. 265, Sep. 2022, Art. no. 111884, doi: [10.1016/J.MEE.2022.111884](https://doi.org/10.1016/J.MEE.2022.111884).
- [132] B. P. Jelle, C. Breivik, and H. Drolsum Røkenes, "Building integrated photovoltaic products: A state-of-the-art review and future research opportunities," *Sol. Energy Mater. Sol. Cells*, vol. 100, pp. 69–96, May 2012, doi: [10.1016/J.SOLMAT.2011.12.016](https://doi.org/10.1016/J.SOLMAT.2011.12.016).
- [133] S. Wang et al., "Bifacial photovoltaic systems energy yield modelling," *Energy Procedia*, vol. 77, pp. 428–433, Aug. 2015, doi: [10.1016/J.EGYPRO.2015.07.060](https://doi.org/10.1016/J.EGYPRO.2015.07.060).
- [134] J. Leaf et al., "Improvement of electrical efficiency in a PV solar farm utilizing agriculture," *AIP Conf. Proc.*, vol. 2635, no. 1, Dec. 2022, Art. no. 70001, doi: [10.1063/5.0105646/2830580](https://doi.org/10.1063/5.0105646/2830580).
- [135] A. D. Cronin et al., "Holographic CPV field tests at the Tucson Electric Power solar test yard," in *Proc. Conf. Rec. IEEE Photovolt. Spec. Conf.*, 2011, pp. 2346–2350, doi: [10.1109/PVSC.2011.6186423](https://doi.org/10.1109/PVSC.2011.6186423).
- [136] T. Simioni and R. Schaeffer, "Georeferenced operating-efficiency solar potential maps with local weather conditions – An application to Brazil," *Sol. Energy*, vol. 184, pp. 345–355, May 2019, doi: [10.1016/J.SOLENER.2019.04.006](https://doi.org/10.1016/J.SOLENER.2019.04.006).
- [137] L. C. Hirst and J. N. Ekins-Daukes, "Fundamental losses in solar cells," *Prog. Photovolt., Res. Appl.*, vol. 19, no. 3, pp. 286–293, May 2009, doi: [10.1002/PIP.1024](https://doi.org/10.1002/PIP.1024).
- [138] S. Ahzi, S. P. Aly, and N. Barth, "New developments in the modeling and simulations of the thermal behavior and electrical yield of photovoltaics panels with the consideration of desert environmental conditions," in *Proc. Int. Renewable Sustain. Energy Conf.*, 2018, pp. 1–6, doi: [10.1109/IRSEC.2017.8477380](https://doi.org/10.1109/IRSEC.2017.8477380).
- [139] S. P. Aly, S. Ahzi, N. Barth, and A. Abdallah, "Using energy balance method to study the thermal behavior of PV panels under time-varying field conditions," *Energy Convers. Manage.*, vol. 175, pp. 246–262, Nov. 2018, doi: [10.1016/J.ENCONMAN.2018.09.007](https://doi.org/10.1016/J.ENCONMAN.2018.09.007).
- [140] "How to achieve the revised IEC 61215 and IEC 61730 certification for Solar PV modules." [Online]. Available: <https://insights.tuv.com/blog/how-to-achieve-revised-iec61215-iec-61730>
- [141] "IEC 61853-1:2011 | IEC webstore | rural electrification, solar power, LVDC." [Online]. Available: <https://webstore.iec.ch/publication/6035>
- [142] "IEC 62790:2020 RLV | IEC Webstore | rural electrification, solar power, LVDC." [Online]. Available: <https://webstore.iec.ch/publication/67338>
- [143] "IEC TS 60904-1-2:2019 | IEC Webstore | water management, smart city, rural electrification, solar power, solar panel, photovoltaic, PV, LVDC." [Online]. Available: <https://webstore.iec.ch/publication/34357>
- [144] "IEC 60891:2021 | IEC Webstore." [Online]. Available: <https://webstore.iec.ch/publication/61766>
- [145] "IEC 62930:2017 | IEC Webstore." [Online]. Available: <https://webstore.iec.ch/publication/28067>
- [146] "IEC 60904-7:2019 | IEC Webstore | water management, smart city, rural electrification, solar power, solar panel, photovoltaic, PV, LVDC." [Online]. Available: <https://webstore.iec.ch/publication/26502>
- [147] "IEC 62852:2014 | IEC Webstore | rural electrification, solar power, LVDC." [Online]. Available: <https://webstore.iec.ch/publication/7463>
- [148] "IEC 60904-9:2020 | IEC Webstore | water management, smart city, rural electrification, solar power, solar panel, photovoltaic." [Online]. Available: <https://webstore.iec.ch/publication/28973>
- [149] W. Herrmann, M. Schweiger, and J. Bonilla, "Performance characteristics of bifacial PV modules and power labeling," in *Proc. BifiPV2017 Workshop*, vol. 25, no. 26, Oct. 2017.
- [150] "Photovoltaic Research News | Photovoltaic Research | NREL." [Online]. Available: <https://www.nrel.gov/pv/news.html?year=2020>
- [151] "Sandia National Laboratories." [Online]. Available: <https://www.sandia.gov/>
- [152] "Global Website - Precisely Right. | WO | TÜV Rheinland." [Online]. Available: <https://www.tuv.com/world/en/>
- [153] "Temperature test series - Haida International Equipment." [Online]. Available: https://www.qtstest.com/products/environmental-test-chamber/temperature-test-series/?gad_source=1&gclid=CjwKCAiAloavBhBOEiwAbtAJO_hmVZ0RDWSHX3n2JrGh_APjXftGWOUKcLSD-Kr8ukUohbWMpbpcBoC_oAQAvD_BwE
- [154] M. D. Kempe, D. Holsapple, K. Whitfield, and N. Shiradkar, "Standards development for modules in high temperature micro-environments," *Prog. Photovolt., Res. Appl.*, vol. 29, no. 4, pp. 445–460, Apr. 2021, doi: [10.1002/PIP.3389](https://doi.org/10.1002/PIP.3389).
- [155] X. Zhang, C. Monokroussos, M. Schweiger, and M. Heinze, "Power rating and qualification of bifacial PV modules," Accessed: Oct. 11, 2023. [Online]. Available: pv-tech.org
- [156] J. Stein et al., "Bifacial photovoltaic modules and systems: Experience and results from international research and pilot applications," Sandia National Lab.(SNL-NM), Albuquerque, NM (United States); Fraunhofer..., 2021.
- [157] M. R. Vogt et al., "Developing an energy rating for bifacial photovoltaic modules," *Prog. Photovolt.*, vol. 31, pp. 1466–1477, 2023, doi: [10.1002/PIP.3678](https://doi.org/10.1002/PIP.3678).
- [158] S. Reichmuth et al., "Measurement uncertainties in I–V calibration of multi-junction solar cells for different solar simulators and reference devices," *IEEE J. Photovolt.*, vol. 10, no. 4, pp. 1076–1083, Jul. 2020.
- [159] R. P. Kenny et al., "Proposal for the extension of the energy rating standard series IEC 61853 to bifacial modules," in *Proc. 8th World Conf. Photovolt. Energy Convers.*, 2022, pp. 724–730, doi: [10.4229/WCPEC-82022-3BV.3.41](https://doi.org/10.4229/WCPEC-82022-3BV.3.41).
- [160] J. Castro, M. Schweiger, D. Moser, and T. Tanahashi, "Climatic rating of photovoltaic modules: Different technologies for various operating conditions," 2020, Accessed: Oct. 11, 2023.
- [161] J. P. Singh, A. G. Aberle, and T. M. Walsh, "Electrical characterization method for bifacial photovoltaic modules," *Sol. Energy Mater. Sol. Cells*, vol. 127, pp. 136–142, Aug. 2014, doi: [10.1016/J.SOLMAT.2014.04.017](https://doi.org/10.1016/J.SOLMAT.2014.04.017).

- [162] J. E. Castillo-Aguilella and P. S. Hauser, "Bifacial photovoltaic module best-fit annual energy yield model with azimuthal correction," in *Proc. Conf. Rec. IEEE Photovolt. Spec. Conf.*, 2016, pp. 3109–3112, doi: [10.1109/PVSC.2016.7750238](https://doi.org/10.1109/PVSC.2016.7750238).
- [163] H. D. M. R. Perera and H. Wen, "Power generation and performance analysis of bi-facial vs mono-facial 10KW photovoltaic power station," in *Proc. 18th Int. Conf. Opt. Commun. Netw.*, 2019, pp. 1–3, doi: [10.1109/ICOCON.2019.8934305](https://doi.org/10.1109/ICOCON.2019.8934305).
- [164] C. Deline et al., "Evaluation and field assessment of bifacial photovoltaic module power rating methodologies," in *Proc. Conf. Rec. IEEE Photovolt. Spec. Conf.*, 2016, pp. 3698–3703, doi: [10.1109/PVSC.2016.7750367](https://doi.org/10.1109/PVSC.2016.7750367).
- [165] R. Kopecek and J. Libal, "Complex problems require simple solutions: How to measure bifacial devices correctly," *pv-tech.org* PV Int., 2017, Accessed: Oct. 11, 2023.
- [166] J. Rodriguez, "Bifacial solar cells—the two sides of the story. Google Scholar," *Sol Choice Pty Ltd*, vol. 44, 2015.
- [167] H. Nussbaumer et al., "New opportunities for a better power distribution by the use of bifacial modules in future PV systems," *présenté à BIFIPV workshop, Chambéry*, 2014.
- [168] M. Nannetti, "Techno-economic assessment of two agrovoltaics case studies," 2022.
- [169] Z. Zhang et al., "The mathematical and experimental analysis on the steady-state operating temperature of bifacial photovoltaic modules," *Renewable Energy*, vol. 155, pp. 658–668, 2023.
- [170] K. McIntosh et al., "Simulation and measurement of monofacial and bifacial modules in a 1D tracking system," in *Proc. IEEE 47th Photovolt. Spec. Conf.*, 2023, pp. 366–370.
- [171] A. Di Stefano, G. Leotta, and F. Bizzarri, "La Silla PV plant as a utility-scale side-by-side test for innovative modules technologies," in *Proc. 33rd Eur. Photovolt. Sol. Energy Conf. Exhib.*, 2017, pp. 1978–1982.
- [172] A. Meguro, H. Ishikawa, and A. Tsujihata, "Study on ground verification for large deployable modular structures," *J. Spacecr Rockets*, vol. 43, no. 4, pp. 780–787, 2006, doi: [10.2514/1.16037](https://doi.org/10.2514/1.16037).
- [173] A. Sahu, N. Yadav, and K. Sudhakar, "Floating photovoltaic power plant: A review," *Renewable Sustain. Energy Rev.*, vol. 66, pp. 815–824, 2016, doi: [10.1016/j.rser.2016.08.051](https://doi.org/10.1016/j.rser.2016.08.051).
- [174] S. Panda et al., "Analyzing and evaluating floating PV systems in relation to traditional PV systems," *Mater. Today, Proc.*, 2023.
- [175] S. Gökmener, E. Oğuz, M. Deveci, and K. Göllü, "Site selection for floating photovoltaic system on dam reservoirs using sine trigonometric decision making model," *Ocean Eng.*, vol. 281, 2023, Art. no. 114820.
- [176] A. El Hammoumi et al., "Design and construction of a test bench to investigate the potential of floating PV systems," *J. Cleaner Prod.*, vol. 278, 2020, Art. no. 123917, doi: [10.1016/j.jclepro.2020.123917](https://doi.org/10.1016/j.jclepro.2020.123917).
- [177] A. Goswami, P. Sadhu, U. Goswami, and P. K. Sadhu, "Floating solar power plant for sustainable development: A techno-economic analysis," *Environ Prog Sustain Energy*, vol. 38, no. 6, Nov. 2019, Art. no. e13268, doi: [10.1002/EP.13268](https://doi.org/10.1002/EP.13268).
- [178] S. Oliveira-Pinto and J. Stokkermans, "Assessment of the potential of different floating solar technologies—Overview and analysis of different case studies," *Energy Convers. Manage.*, vol. 211, 2023, Art. no. 112747.
- [179] V. Ramasamy and R. Margolis, "Floating photovoltaic system cost benchmark: Q1 2021 installations on artificial water bodies," Tech. Rep. NREL/TP-7A40-80695, Nat. Renewable Energy Lab., Golden, CO, USA, 2021, Accessed: Oct. 12, 2023.
- [180] S. Guo, T. M. Walsh, and M. Peters, "Vertically mounted bifacial photovoltaic modules: A global analysis," *Energy*, vol. 61, pp. 447–454, Nov. 2013, doi: [10.1016/J.ENERGY.2013.08.040](https://doi.org/10.1016/J.ENERGY.2013.08.040).
- [181] L. Koskinen, "Vertical bifacial photovoltaic system," 2019.
- [182] M. R. Khan, A. Hanna, X. Sun, and M. A. Alam, "Vertical bifacial solar farms: Physics, design, and global optimization," *Appl. Energy*, vol. 206, pp. 240–248, Nov. 2017, doi: [10.1016/J.APENERGY.2017.08.042](https://doi.org/10.1016/J.APENERGY.2017.08.042).
- [183] D. Chudinow, J. Haas, G. Díaz-Ferrán, S. Moreno-Leiva, and L. Eltrop, "Simulating the energy yield of a bifacial photovoltaic power plant," *Sol. Energy*, vol. 183, pp. 812–822, 2023.
- [184] F. Bosatelli et al., "Enel green power's AI tool for anomaly detection on PV plant thermographies collected with UAS," in *Proc. IEEE Int. Conf. Environ. Electr. Eng., IEEE Ind. Commercial Power Syst. Europe*, 2021, pp. 1–3.
- [185] F. Giordano, Z. Tulumen, R. Sanchez, and G. Magnacca, "White roof as a multiple benefits low-cost technology: A state of the art," *CERN IdeaSquare J. Exp. Innov.*, vol. 3, no. 2, pp. 12–17, Dec. 2019, doi: [10.23726/CJ.2019.874](https://doi.org/10.23726/CJ.2019.874).
- [186] A. Grigorescu, V. L. Ruiz, C. Lincaru, and E. C. Condrea, "Specialization patterns for the development of renewable energy generation technologies across countries," *Energies*, vol. 16, 2023, Art. no. 7164, doi: [10.3390/en16207164](https://doi.org/10.3390/en16207164).
- [187] A. Thompson, "Modular water harvester ensures continuous water production for arid regions," *Scilight*, vol. 2023, 2023, Art. no. 461101.
- [188] W. Wu et al., "Development of industrial n-type bifacial topcon solar cells and modules," in *Proc. 37th Eur. Photovolt. Sol. Energy Conf. Exhib.*, doi: [10.4229/EUPVSEC20192019-2BP.1.5](https://doi.org/10.4229/EUPVSEC20192019-2BP.1.5).
- [189] J. Joubert et al., "Performance evaluation of bifacial and monofacial modules in vertical and latitude mounting at South India using PVsyst," *IOP Conf. Ser. Mater. Sci. Eng.*, vol. 912, no. 4, Aug. 2020, Art. no. 042066, doi: [10.1088/1757-899X/912/4/042066](https://doi.org/10.1088/1757-899X/912/4/042066).
- [190] K.-J. Cho and D.-W. Cho, "Experimental analysis on annual power generations of louver-integrated bi-facial photovoltaic modules for architectural applications," *J. Korean Sol. Energy Soc.*, vol. 42 pp. 47–56, Feb. 2022, doi: [10.7836/KSES.2022.42.1.047](https://doi.org/10.7836/KSES.2022.42.1.047).
- [191] H. Nussbaumer et al., "Accuracy of simulated data for bifacial systems with varying tilt angles and share of diffuse radiation," *Sol. Energy*, vol. 197, pp. 6–21, Feb. 2020, doi: [10.1016/J.SOLENER.2019.12.071](https://doi.org/10.1016/J.SOLENER.2019.12.071).
- [192] M. Ernst, G. E. J. Conechado, and C. A. Asselineau, "Accelerating the simulation of annual bifacial illumination of real photovoltaic systems with ray tracing," *iScience*, vol. 25, no. 1, Jan. 2022, Art. no. 103698, doi: [10.1016/J.ISCI.2021.103698](https://doi.org/10.1016/J.ISCI.2021.103698).
- [193] S. Bouchakour et al., "Modelling and simulation of bifacial PV production using monofacial electrical models," *Energies*, vol. 14, Jul. 2021, Art. no. 4224, doi: [10.3390/EN14144224](https://doi.org/10.3390/EN14144224).
- [194] P. M. Jansson, M. G. Newberry, and S. M. Myers, "Agrivoltaics using bi-facial PVs for permaculture in utility-scale projects," in *Proc. Conf. Rec. IEEE Photovolt. Spec. Conf.*, 2022, pp. 330–332, doi: [10.1109/PVSC48317.2022.9938476](https://doi.org/10.1109/PVSC48317.2022.9938476).
- [195] A. Skumanich and M. Ghiasi, "The need for AI to optimize dual-use PV installations to extract maximum value," in *Proc. Conf. Rec. IEEE Photovolt. Spec. Conf.*, 2021, pp. 459–463, doi: [10.1109/PVSC43889.2021.9518677](https://doi.org/10.1109/PVSC43889.2021.9518677).
- [196] O. A. Katsikogiannis, H. Ziar, and O. Isabella, "Integration of bifacial photovoltaics in agrivoltaic systems: A synergistic design approach," *Appl. Energy*, vol. 309, Mar. 2022, Art. no. 118475, doi: [10.1016/J.APENERGY.2021.118475](https://doi.org/10.1016/J.APENERGY.2021.118475).
- [197] S. Amaducci, X. Yin, and M. Colauzzi, "Agrivoltaic systems to optimise land use for electric energy production," *Appl. Energy*, vol. 220, pp. 545–561, Jun. 2018, doi: [10.1016/J.APENERGY.2018.03.081](https://doi.org/10.1016/J.APENERGY.2018.03.081).
- [198] G. A. Barron-Gafford et al., "Agrivoltaics provide mutual benefits across the food–energy–water nexus in drylands," *Nature Sustain.*, vol. 2, no. 9, pp. 848–855, Sep. 2019, doi: [10.1038/s41893-019-0364-5](https://doi.org/10.1038/s41893-019-0364-5).
- [199] J. Cho et al., "Application of photovoltaic systems for agriculture: A study on the relationship between power generation and farming for the improvement of photovoltaic applications in agriculture," *Energies*, vol. 13, no. 18, Sep. 2020, Art. no. 4815, doi: [10.3390/EN13184815](https://doi.org/10.3390/EN13184815).
- [200] M. Cossu et al., "Solar radiation distribution inside a greenhouse with south-oriented photovoltaic roofs and effects on crop productivity," *Appl. Energy*, vol. 133, pp. 89–100, Nov. 2014, doi: [10.1016/J.APENERGY.2014.07.070](https://doi.org/10.1016/J.APENERGY.2014.07.070).
- [201] C. Dupraz et al., "Combining solar photovoltaic panels and food crops for optimising land use: Towards new agrivoltaic schemes," *Renewable Energy*, vol. 36, no. 10, pp. 2725–2732, Oct. 2011, doi: [10.1016/J.RENENE.2011.03.005](https://doi.org/10.1016/J.RENENE.2011.03.005).
- [202] A. Leon and K. N. Ishihara, "Assessment of new functional units for agrivoltaic systems," *J. Environ. Manage.*, vol. 226, pp. 493–498, Nov. 2018, doi: [10.1016/J.JENVMAN.2018.08.013](https://doi.org/10.1016/J.JENVMAN.2018.08.013).
- [203] H. Marrou, J. Wery, L. Dufour, and C. Dupraz, "Productivity and radiation use efficiency of lettuces grown in the partial shade of photovoltaic panels," *Eur. J. Agronomy*, vol. 44, pp. 54–66, Jan. 2013, doi: [10.1016/J.EJA.2012.08.003](https://doi.org/10.1016/J.EJA.2012.08.003).
- [204] "InSPIRE | Open Energy Information." [Online]. Available: <https://openei.org/wiki/InSPIRE>
- [205] B. Beatty, J. Macknick, J. McCall, G. Braus, and D. Buckner, "Native vegetation performance under a Solar PV array at the National Wind Technology Center," Tech. Rep. NREL/TP-1900-66218, Nat. Renewable Energy Lab., Golden, CO, USA, May 2017, doi: [10.2172/135787](https://doi.org/10.2172/135787).
- [206] J. Macknick et al., "The 5 Cs of agrivoltaic success factors in the United States: Lessons from the InSPIRE research study," Tech. Rep. NREL/TP-6A20-83566, Nat. Renewable Energy Lab., Golden, CO, USA, Aug. 2022, doi: [10.2172/1882930](https://doi.org/10.2172/1882930).

- [207] H. Marrou, L. Dufour, and J. Wery, "How does a shelter of solar panels influence water flows in a soil–crop system?", *Eur. J. Agronomy*, vol. 50, pp. 38–51, Oct. 2013, doi: [10.1016/J.EJA.2013.05.004](https://doi.org/10.1016/J.EJA.2013.05.004).
- [208] M. Trommsdorff et al., "Combining food and energy production: Design of an agrivoltaic system applied in arable and vegetable farming in Germany," *Renewable Sustain. Energy Rev.*, vol. 140, Apr. 2021, Art. no. 110694, doi: [10.1016/J.RSER.2020.110694](https://doi.org/10.1016/J.RSER.2020.110694).
- [209] M. A. Al Mamun, P. Dargusch, D. Wadley, N. A. Zulkarnain, and A. A. Aziz, "A review of research on agrivoltaic systems," *Renewable Sustain. Energy Rev.*, vol. 161, Jun. 2022, Art. no. 112351, doi: [10.1016/J.RSER.2022.112351](https://doi.org/10.1016/J.RSER.2022.112351).
- [210] L. W. Farrar, A. B. S. Bahaj, P. James, A. Anwar, and N. Amdar, "Floating solar PV to reduce water evaporation in water stressed regions and powering water pumping: Case study Jordan," *Energy Convers. Manage.*, vol. 260, May 2022, Art. no. 115598, doi: [10.1016/J.ENCONMAN.2022.115598](https://doi.org/10.1016/J.ENCONMAN.2022.115598).
- [211] M. Kumar, H. M. Niyaz, and R. Gupta, "Challenges and opportunities towards the development of floating photovoltaic systems," *Sol. Energy Mater. Sol. Cells*, vol. 233, Dec. 2021, Art. no. 111408, doi: [10.1016/J.SOLMAT.2021.111408](https://doi.org/10.1016/J.SOLMAT.2021.111408).
- [212] H. Liu, A. Kumar, and T. Reindl, "The dawn of floating solar—Technology, benefits, and challenges," *Lecture Notes Civil Eng.*, vol. 41, pp. 373–383, 2020, doi: [10.1007/978-981-13-8743-2_21_COVER](https://doi.org/10.1007/978-981-13-8743-2_21_COVER).
- [213] J. Agnelli, A. Dib, A. Pierattini, and N. Fantuzzi, "Feasibility study of floating photovoltaic panels in the Adriatic Sea," in *Proc. IEEE Int. Conf. Environ. Electr. Eng., IEEE Ind. Commercial Power Syst. Europe*, 2023, pp. 1–6, doi: [10.1109/EEEIC/ICPSEUROPE57605.2023.10194722](https://doi.org/10.1109/EEEIC/ICPSEUROPE57605.2023.10194722).
- [214] A. N. Gajudhur, "Solar PV options to reduce emissions from drilling, completions, and production operations," 2022.
- [215] Y. A. Mistry and S. N. Khandekar, "Analysis of Solar photovoltaic technologies integrated with storage systems and fuel cell vehicle," *ECS Trans.*, vol. 107, no. 1, pp. 16707–16723, Apr. 2022, doi: [10.1149/10701.16707ECST/XML](https://doi.org/10.1149/10701.16707ECST/XML).
- [216] T. M. Mahim, A. H. M. A. Rahim, and M. M. Rahman, "Prediction of custom-built bi-facial PV panel output including weather parameters," in *Proc. 12th Int. Conf. Renewable Energy Res. Appl.*, 2023, pp. 219–224, doi: [10.1109/ICRERA59003.2023.10269448](https://doi.org/10.1109/ICRERA59003.2023.10269448).
- [217] M. R. M. F. Barros E Silva et al., "A study about solar tracker for the performance of photovoltaic plants," in *Proc. 6th Int. Symp. Instrum. Syst., Instrum. Syst., Circuits Transducers*, Porto Alegre, Brazil, pp. 1–6, 2022, doi: [10.1109/INSCIT55544.2022.9913749](https://doi.org/10.1109/INSCIT55544.2022.9913749).
- [218] A. C. J. Russell, C. E. Valdivia, C. Bohemier, J. E. Haysom, and K. Hinzer, "DUET: A novel energy yield model with 3-D shading for bifacial photovoltaic systems," *IEEE J. Photovolt.*, vol. 12, no. 6, pp. 1576–1585, Nov. 2022, doi: [10.1109/JPHOTOV.2022.3185546](https://doi.org/10.1109/JPHOTOV.2022.3185546).
- [219] S. Sreenath, K. Sudhakar, and A. F. Yusop, "Performance assessment of conceptual bifacial solar PV system in varying albedo conditions," *IOP Conf. Ser. Mater. Sci. Eng.*, vol. 1078, no. 1, Feb. 2021, Art. no. 012033, doi: [10.1088/1757-899X/1078/1/012033](https://doi.org/10.1088/1757-899X/1078/1/012033).
- [220] S. A. Kalhoro, S. H. Abbas Musavi, S. Ali, S. Rahoojo, and A. Nawaz, "An economical and relatively efficient implementation of the real-time solar tracking system," *3c Tecnología: Glosas de Innovación Aplicadas a la Pyme*, vol. 8, no. 1, pp. 68–99, 2019, doi: [10.17993/3ctecno.2019.specialissue2.68-99](https://doi.org/10.17993/3ctecno.2019.specialissue2.68-99).
- [221] "Home - system Advisor model - SAM." [Online]. Available: <https://sam.nrel.gov/>
- [222] T. Tezer, R. Yaman, and G. Yaman, "Evaluation of approaches used for optimization of stand-alone hybrid renewable energy systems," *Renewable Sustain. Energy Rev.*, vol. 73, pp. 840–853, 2017, doi: [10.1016/j.rser.2017.01.118](https://doi.org/10.1016/j.rser.2017.01.118).
- [223] C. D. Rodríguez-Gallegos et al., "Global techno-economic performance of bifacial and tracking photovoltaic systems," *Joule*, vol. 4, no. 7, pp. 1514–1541, Jul. 2020, doi: [10.1016/J.JOULE.2020.05.005](https://doi.org/10.1016/J.JOULE.2020.05.005).
- [224] "Intersolar South America - Home - Intersolar South America." [Online]. Available: <https://www.intersolar.net.br/home>
- [225] "SNEC 16th (2022) International Photovoltaic Power Generation and Smart Energy Conference and Exhibition," Zhejiang Hecheng Electric Co., Ltd., Hangzhou, China, Accessed: Aug. 26, 2023.
- [226] M. Aghaei et al., "Bifacial photovoltaic technology: Recent advancements, simulation and performance measurement," in *Solar Radiation - Measurement, Modeling and Forecasting Techniques for Photovoltaic Solar Energy Applications*. London, U.K.: IntechOpen, 2022, doi: [10.5772/INTECHOPEN.105152](https://doi.org/10.5772/INTECHOPEN.105152).
- [227] PV Power, Inc., Company profile and news - Bloomberg Markets, Accessed: Aug. 26, 2023.
- [228] T. Dannenberg et al., "Past, present, and future outlook for edge isolation processes in highly efficient silicon solar cell manufacturing," *Sol. RRL*, vol. 7, no. 8, Apr. 2023, Art. no. 2200594, doi: [10.1002/SOLR.202200594](https://doi.org/10.1002/SOLR.202200594).
- [229] H. Abubakr, J. C. Vasquez, K. Mahmoud, M. M. F. Darwisch, and J. M. Guerrero, "Comprehensive review on renewable energy sources in Egypt-current status, grid codes and future vision," *IEEE Access*, vol. 10, pp. 4081–4101, 2022, doi: [10.1109/ACCESS.2022.3140385](https://doi.org/10.1109/ACCESS.2022.3140385).